Bayesian interface based calibration of a novel rockfall protection structure modelled in the Non-smooth contact dynamics framework

Ritesh Gupta, Franck Bourrier, Vincent Acary, Stéphane Lambert

▶ **To cite this version:**

Ritesh Gupta, Franck Bourrier, Vincent Acary, Stéphane Lambert. Bayesian interface based calibration of a novel rockfall protection structure modelled in the Non-smooth contact dynamics framework. Engineering Structures, 2023, 10.1016/j.engstruct.2023.116936 . hal-04039263v1

HAL Id: hal-04039263

https://hal.science/hal-04039263v1

Submitted on 21 Mar 2023 (v1), last revised 13 Oct 2023 (v2)

HAL is a multi-disciplinary open access archive for the deposit and dissemination of scientific research documents, whether they are published or not. The documents may come from teaching and research institutions in France or abroad, or from public or private research centers.

L'archive ouverte pluridisciplinaire **HAL**, est destinée au dépôt et à la diffusion de documents scientifiques de niveau recherche, publiés ou non, émanant des établissements d'enseignement et de recherche français ou étrangers, des laboratoires publics ou privés.

Distributed under a Creative Commons Attribution 4.0 International License

Bayesian interface based calibration of a novel rockfall protection structure modelled in the Non-smooth contact dynamics framework

Ritesh Gupta[a,*], Franck Bourrier[a,b], Vincent Acary[b], Stéphane Lambert[a]

[a] *Univ. Grenoble Alpes, INRAE, CNRS, IRD, Grenoble INP, IGE, 38000 Grenoble, France*
[b] *Univ. Grenoble Alpes, Inria, CNRS, Grenoble INP, Institute of Engineering, LJK, 38000 Grenoble, France*

Abstract

This article presents the development and calibration of a numerical model simulating the response of large structure to a localized dynamic loading. A novel rockfall protection structure composed of piled up concrete blocks interconnected via metallic components is studied, where the underlying intricacies are revealed by real-scale impact experiments. The numerical model is developed using the Siconos software based on the Non-Smooth Contact Dynamics (NSCD) method to further investigate the efficiency and performance of this new structure type. All geometrical features and mechanical properties of the real structure components are incorporated via specific developments pertinent to the modeling requirements in Siconos. Some parameters peculiar to the numerical model are calibrated against the spatial-temporal measurements from two full-scale impact experiments. The Bayesian interface statistical learning method aided by the polynomial chaos expansion based meta-model of the NSCD model is deployed for the calibration. The additional understanding of the model dynamics through the byproducts of meta-model are highlighted. In the end, the NSCD model is successfully calibrated against the spatial-temporal response of the experimental structure for impact energies up to 1 MJ.

Keywords: rockfall, impact, meta-model, statistical learning, NSCD modeling, calibration, Bayesian interface

1. Introduction

The Non-Smooth Contact Dynamics (NSCD) approach was developed to solve multi-body multi-contact problems with rigid and/or deformable bodies [1, 2, 3, 4]. It finds many modeling application in the field of civil engineering and geomechanics such as; masonry and stone structures exposed to static, cyclic and dynamic loading [5, 6, 7]; cohesive and non-cohesive granular materials [8, 9]; and rockfall

*Corresponding author
Email address: ritesh.gupta@inrae.fr (Ritesh Gupta)

propagation on slopes [10] in particular. All these applications consider bodies interacting with each other via surface contacts. Hence, NSCD approach can also be used for mechanisms and linkages [11] and has also been easily combined with standard Finite Element Method (FEM) from the early stage of its development [12, 13].

The present work extends the use of NSCD modeling for the impact study on a complex structure made of individual concrete blocks interconnected one to the other via metallic components, thus forming an articulated structure. These types of structures are proposed by the company Géolithe and are intended to serve as passive protection against gravity driven natural hazards. It is in particular designed to intercept rockfall, similarly as other massive structure types including embankments [14, 15, 16, 17], concrete walls [18, 19, 20], concrete blocks cushioned with gabions [21, 22, 23], gabion structures [24] and sea containers [25]. This innovative technology offers the possibility to build massive vertical walls, with reduced foot print, high deformability and versatility.

The development of this technology is based on small-scale experiments, to address the structure response considering different design options [26], and real-scale impact experiments to demonstrate the structure capacity in arresting rock blocks with kinetic energy exceeding 1 MJ [27]. These experiments revealed the intricacy of the impact response of structures made from interconnected concrete blocks. The impact induces sliding at the base and tilting of the structure, where the amplitude depends on the impact energy and distance to the impact point [26]. In addition, interconnection between concrete blocks improve the structure stability preventing from excessive concrete blocks displacements in the impact vicinity.

The impact response of small- and real-scale structures has been previously investigated in the numerical modeling framework of the finite volume formulation code FLAC3D [26, 27]. These models provided the detailed insights on the energy dissipation capacities of the protection walls. However, the computation time for real-scale structure ranging from 10 to 20 hours hinders the exhaustive investigations of the structure mechanical and dynamic response. In particular, improving the design of such structures requires better quantifying their efficiency when exposed to rockfall. In line with some previous research on flexible barriers [28, 29, 30], this implies taking into account the variety of loading cases observed during real rockfalls and therefore performing a very large number of simulations of the structure's response to the impact.

Given the above, the authors developed a NSCD-based model of the structure, using the SICONOS software [31, 32]. SICONOS is an open-source scientific software primarily targeted at modeling and simulating non-smooth dynamical systems in C++ and in Python, including mechanical systems, switched electrical circuits, sliding mode control systems and biology. The NSCD method guarantees that the Signorini's condition at the velocity level is satisfied without introducing contact stiffnesses, and that the coulomb friction, especially in the sticking mode is satisfied without resorting to viscous friction. This peculiarity of NSCD is enforced with the use of a specific implicit scheme (Moreau–Jean scheme) and yields a robust numerical method, which consistently models the threshold phenomena (friction, contact) and the dissipation properties of the model in discrete time, in particular impact dissipation and energy properties [33].

Considering its intended use, the developed model is kept as simple as possible while allowing satisfactorily mimicking the whole structure's response to impact, as observed during the real-scale experiments. Such simplifications drastically reduce the computational time as each component of the structure is modeled as a rigid body instead of a deformable mesh resulting in a huge reduction in the degrees of freedom of the model. The energy dissipation due to plastic strains and breakages of the blocks during impact is modeled in a simple manner as energy dissipation at the contact points. Escallón et al. [34] reported a conceptually similar approach for the FEM model of flexible rockfall protection barriers and observed a significant reduction in the model computational time.

Further, the calibration of model parameters becomes necessary to validate the model performance. For this, an existing experimental database [27] is used as a reference and some identified model parameters are calibrated using Bayesian interface method. This method belongs to the category of parameters identification through inverse formulation [34, 35] and a calibration technique [36, 37] extensively used to reproduce the experimental or practical observations through optimum model parameters identification. It statistically learns the trends of the model output response on the large dataset of the model input parameters as per the recorded experimental observations.

A common requirement of any stochastic method is a large number of model computations for reliability and abiding with the law of the large numbers and the central limit theorems. Therefore, even after a significant reduction in model computation time (say to within a few minutes), the stochastic methods continue to be impractical to implement due to a large computation cost. This gap is bridged

by the use of meta-model, representative of the actual model having a negligible computational cost and possess high accuracy and reliability. Such meta-models (or surrogate models) have been used by many researchers, *e.g.,* for dam engineering problems [38, 39] and for nuclear containment structures [40].

In the present work, the NSCD-based model is first described in detail, including specific developments to cope with the particular features of this structure type. A polynomial chaos expansion-based meta-model of the NSCD model is created for the stochastic analysis. The additional byproduct of PCE based meta-models towards the relative influence of model parameters is discussed. The model parameters are calibrated based on the Bayesian interface approach considering the measurements obtained from two impact experiments. A discussion on model features in line with the perspectives for the future research concludes the work.

2. Experimental structure and its impact response

The considered articulated structures consist in piled up blocks, made from concrete and are reinforced with steel rebars [27], presented in Figure 1. The block extremities in the horizontal plane are rounded and their upper and lower faces present empty spaces. The wall is made up of 38 blocks and four half-blocks stacked in four rows. The blocks are arranged following a zig-zag pattern (at 45° angle) to improve the structure stability vs titling. The wall is 3.2 m in height and about 14 m in length.

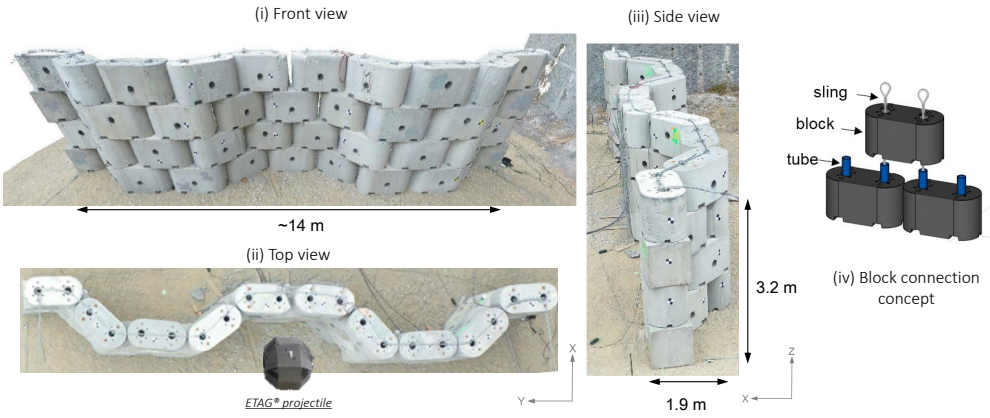

Figure 1: Experimental full-scale structure, modified after [27]

Each block is traversed by two cylindrical holes of diameter 154mm along the vertical axis to receive tubes and slings. These latter metallic components, hereafter referred to as connectors, link blocks together. More precisely, a hollow steel tube of diameter 139.7mm connects each couple of superimposed

blocks, preventing from their relative displacements along the horizontal direction. In addition, a cable runs from the structure base to its top, in the succession of tubes, and mainly prevents from relative displacements along the vertical direction. On a conceptual point of view, these connectors provide the structure with mechanical continuity with the aim of increasing the number of blocks involved in the structure's response proportional to the impact loading. Another key feature in the design is the presence of various plays : a 40 mm distance between adjacent concrete blocks, an approx. 14 mm difference between the external diameter of the metallic tubes and the inner diameter of the cylindrical holes and, a slack in the vertical cables [27]. These plays give the structure a certain deformation capacity. All geometrical and mechanical characteristics of this structure are presented in Table 1 along with the ones of the impacting projectile.

Table 1: Geometrical and mechanical characteristics of the articulated concrete blocks structure

Component	Parameter	Value	Unit
Concrete Block	Length	1.56	m
	Width	0.76	m
	Height	0.80	m
	Mass (m_{block})	1800	kg
	Hole diameter	154	mm
Cylindrical bars	Diameter (ext.)	139.7	mm
	Diameter (int.)	123.7	mm
	Length	0.8 (3 pcs.)	m
		0.4 (2 pcs.)	m
Structure	Length (edge-to-edge)	≈14	m
	Height	3.2	m
	Pattern angle	45 (from y-axis)	°
Projectile	Side length (l_{proj})	1.1	m
	Mass (m_{proj})	2600	kg
	Impact angle	0	°
	Impact point location	y ≈ 7.0, z = 1.7	m

Two identical real-scale walls where built and submitted to one impact each. The impact experiments were performed with the pendulum testing facility of the Université Gustave Eiffel test site (Montagnole, France). It involved a 2600 kg in mass reinforced concrete projectile which shape is in accordance with the requirements for flexible barriers testing (EOTA 2018). Its size is about one-third the structure height (1.1 m). The velocity at impact is 20m/s and 28m/s during the first and second impacts, corresponding to kinetic energies of 520 and 1020 kJ respectively. The angle of incidence and rotation velocity at impact were zero. The projectile impacted the structure at its mid-length and at about 1.7m from the ground. These impacts in particular induced wall sliding at its base, tilting, change in conformation as well as concrete blocks damage.

The structure impact response with time is described based on measurements of displacement and acceleration along two vertical lines, as presented in Figure 2. They are termed as impact and distant axis which are the representative of the impact point and 3.5m to its left respectively. The experimental data used in this study concerned the concrete blocks at the top and at the base in the impact axis and points C and D in the distant distant axis. Besides, the data from two points A and B in the impact axis is also available which is used for the cross-reference purpose only. Further details on the experiments and data are given in [27].

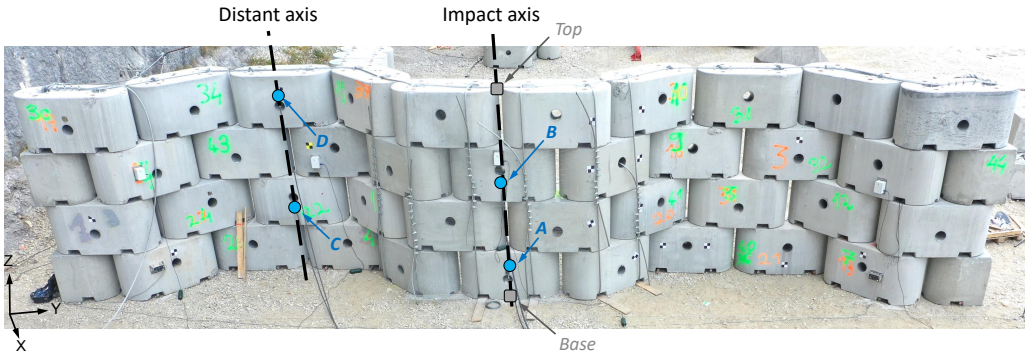

Figure 2: Data acquisition locations in the experimented full-scale structure, recreated after [27]

The displacement governs the structure sliding and tilting and thereby, both leading to structure failure if in excess. Thereby, in this study, only the database of displacement evolution with time in both the impact vicinity and at distance are considered. The displacement data used in this study are plotted in Figure 3 for both impact tests and distant axis. A secondary y-axis is added for distant axis albeit to the relatively low displacement amplitude comparing to the impact axis.

Measures along the impact axis are derived from video records while measures from cable extensome-

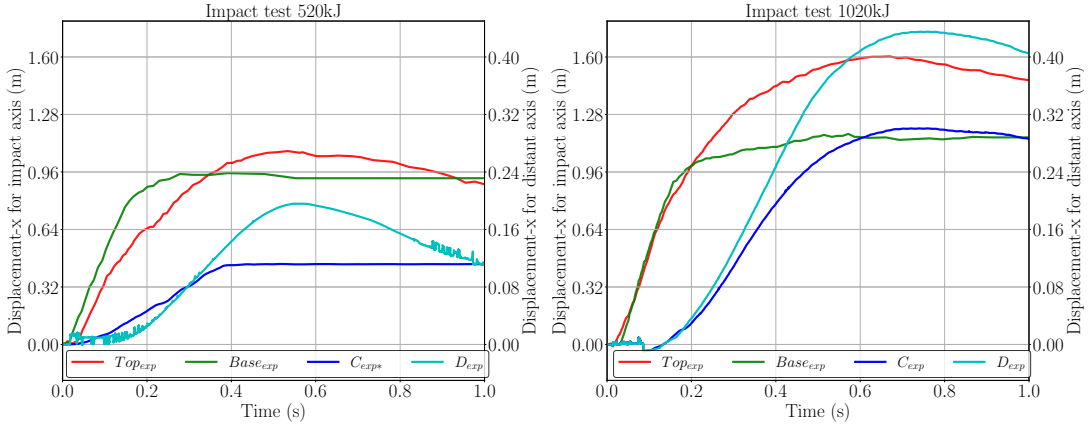

Figure 3: Post-processed experimental database for the time evolution of Displacement for (a) 520 kJ and (b) 1020kJ impact test

ters are considered along the distant axis. Due to the absence of this later data for the 520 kJ impact test at point C, the evolution obtained from simulations presented in [27] are considered. This exception is thought to have minor influence due to the very small amplitude in displacement observed in this specific case. The dynamic response of the structure is clearly visible through the relative initiation time lag between observations corresponding to impact and distant axes.

3. Numerical model

The rockfall protection structure is modeled in a python based software package named Siconos, which implements the NSCD method with complex geometries [31]. The model is developed in the aim of reproducing the whole structure displacement response upon impact by a projectile. In this section, first the constitutive framework of NSCD approach is presented followed by the development of the numerical model in Siconos.

3.1. NSCD main principles and specific features available in Siconos

The Non-Smooth Contact Dynamics (NSCD) method developed by M. Jean and J.J. Moreau [1, 2] is a modeling and numerical framework for the dynamics of multi-body systems in interaction through frictional contact interfaces. In our context, the system is modeled as a collection of rigid blocks connected by unilateral constraints with Coulomb friction. The main feature of the NSCD method is that it can deal with rigid or flexible bodies with rigid contact laws such as the Signorini's model of unilateral contact

and the Coulomb's dry friction without any kind of regularization (viscous friction) or compliance. The finite-freedom dynamics of rigid bodies with unilateral constraints is know to be non-smooth, in the sense that the velocities of the system possesses jumps when a contact is closing with a positive relative velocity. These velocity jumps call for the introduction of an impact law. The NSCD method is able to perform the numerical time integration of the multi-body system with impacts in the dynamics. In this section, we give the main ingredients of the NSCD method referring to the following references for more details [3, 4].

3.1.1. Newton-Euler equations

The configuration of each rigid body in three dimension is described by the position of its center of mass $x_{\mathrm{g}} \in I\!R^3$ and the orientation of the body-fixed frame with respect to a given inertial frame $R \in SO^+(3)$. The velocity of the body is given by the velocity of the center of mass $v_{\mathrm{g}} = \dot{x}_{\mathrm{g}} \in I\!R^3$ and the angular velocity of the body expressed in the body–fixed frame $\Omega \in I\!R^3$. A possible formulation of the Newton-Euler equations of motion for each body is

$$\left\{\begin{array}{rcl} m\,\dot{v}_{\mathrm{g}} & = & f(t, x_{\mathrm{g}}, v_{\mathrm{g}}, R, \Omega) \\ I\dot{\Omega} + \Omega \times I\Omega & = & M(t, x_{\mathrm{g}}, v_{\mathrm{g}}, R, \Omega) \\ \dot{x}_{\mathrm{g}} & = & v_{\mathrm{g}} \\ \dot{R} & = & R\widetilde{\Omega} \end{array}\right. \tag{1}$$

where $m > 0$ is the mass, $I \in I\!R^{3\times 3}$ is the matrix of moments of inertia around the center of mass and the axis of the body–fixed frame, and $f(\cdot) \in I\!R^3$, respectively $M(\cdot) \in I\!R^3$, are the total forces and respectively torques with respect to the center of gravity applied to the body. The matrix $\widetilde{\Omega} \in I\!R^{3\times 3}$ is given by $\widetilde{\Omega}x = \Omega \times x$ for all $x \in I\!R^3$. In the implementation of SICONOS, the orientation matrix R is parameterized by a unit quaternion p such that $R = \Phi(p)$. In the equations of motion (Equation 1), the occurrences of R are substituted by their corresponding expressions in terms of p. The differential equation of Lie type $\dot{R} = R\widetilde{\Omega}$ is replaced by $\dot{p} = \Psi(p)\Omega$ in the unit quaternion space. The closed formulae for Φ and Ψ can be found in any textbook on rigid body dynamics. We denote by q the vector of coordinates of the position and the orientation of the body, and by v the body twist. In matrix notation,

the relation between the body twist v and the time derivative of q is

$$q \coloneqq \begin{bmatrix} x_{\mathrm{g}} \\ p \end{bmatrix}, \quad v \coloneqq \begin{bmatrix} v_{\mathrm{g}} \\ \Omega \end{bmatrix}, \qquad \dot{q} = \begin{bmatrix} \dot{x}_{\mathrm{g}} \\ \Psi(p)\Omega \end{bmatrix} = \begin{bmatrix} I & 0 \\ 0 & \Psi(p) \end{bmatrix} v \coloneqq T(q)v \tag{2}$$

with $T(q) \in \mathbb{R}^{7\times 6}$. A compact matrix form of the Newton Euler equations is

$$\begin{cases} \dot{q} = T(q)v, \\ M\dot{v} = F(t,q,v), \end{cases} \tag{3}$$

where $M \in \mathbb{R}^{6\times 6}$ is the total inertia matrix and $F(t,q,v) \in \mathbb{R}^6$ collects all the forces and torques applied to the body given by

$$M \coloneqq \begin{pmatrix} mI_{3\times 3} & 0 \\ 0 & I \end{pmatrix}, \qquad F(t,q,v) \coloneqq \begin{pmatrix} f(t, x_{\mathrm{g}}, v_{\mathrm{g}}, R, \Omega) \\ I\Omega \times \Omega + M(t, x_{\mathrm{g}}, v_{\mathrm{g}}, R, \Omega) \end{pmatrix}. \tag{4}$$

In the sequel, we assume that the vectors $q \in \mathbb{R}^{7n}$ and $v \in \mathbb{R}^{6n}$ collect the configuration parameters and the velocities of the n bodies in the model. The equation of motion (Equation 3) is rearranged accordingly.

3.1.2. Contact modeling as unilateral constraints and Coulomb friction

For two contacting bodies A and B, we assume that we are able to define one or more contact pair composed of two candidate contact points C_A and C_B and a local frame at contact $(C_A, \mathsf{N}, \mathsf{T}_1, \mathsf{T}_2)$ (see Figure 4 for details). In this local frame, the normal gap function g_{N} is defined as the signed distance between the point C_A and C_B, that is $g_{\mathrm{N}} = (C_B - C_A).\mathsf{N}$. The unilateral contact is given by the Signorini's condition as

$$0 \leqslant g_{\mathrm{N}} \perp r_{\mathrm{N}} \geqslant 0, \tag{5}$$

where r_{N} is the local contact normal force. The symbol $g_{\mathrm{N}} \perp r_{\mathrm{N}}$ means that $g_{\mathrm{N}} r_{\mathrm{N}} = 0$. If the contact is open $g_{\mathrm{N}} > 0$, the contact force r_{N} has to be equal to zero. If the contact is closed $g_{\mathrm{N}} = 0$, then the contact force is nonnegative $r_{\mathrm{N}} \geqslant 0$. As we said before, the dynamics of finite dimensional system requires the definition of an impact law. Let consider the relative velocity u_{N} defined by $u_{\mathrm{N}} = \dot{g}_{\mathrm{N}}$. One of the simplest impact is the Newton impact law given by

$$u_{\mathrm{N}}^{+} = -e u_{\mathrm{N}}^{-}, \text{ if } g_{\mathrm{N}} = 0 \text{ and } u_{\mathrm{N}}^{-} \leqslant 0, \tag{6}$$

where $e \in [0,1]$ is the coefficient of restitution, u_{N}^{+} is the post-impact velocity and u_{N}^{-} the pre-impact velocity.

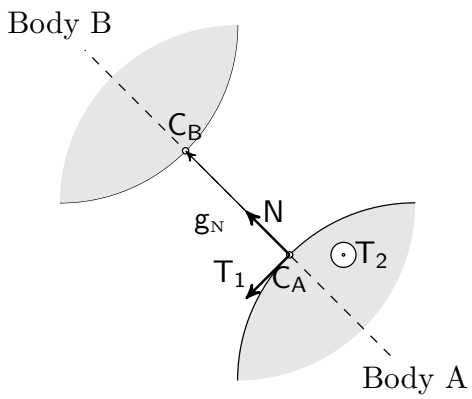

Figure 4: A contact pair and a local contact frame

For the tangential behavior of interface, we consider the Coulomb friction that can be formulated with the Signorini's condition at the velocity level and in terms of the complete reaction forces $r = [r_{\mathrm{N}}, r_{\mathrm{T}}]^\top$ and the relative velocity $u = [u_{\mathrm{N}}, u_{\mathrm{T}}]^\top$ as

$$\begin{cases} r = 0 & \text{if } g_{\mathrm{N}} > 0 \quad \text{(no contact)} \\ r = 0, u_{\mathrm{N}} \geqslant 0 & \text{if } g_{\mathrm{N}} = 0 \qquad \text{(take-off)} \\ r \in K, u = 0 & \text{if } g_{\mathrm{N}} = 0 \qquad \text{(sticking)} \\ r \in \partial K, u_{\mathrm{N}} = 0, \|u_{\mathrm{T}}\| r_{\mathrm{T}} = \|r_{\mathrm{T}}\| u_{\mathrm{T}} & \text{if } g_{\mathrm{N}} = 0 \qquad \text{(sliding)} \end{cases} \tag{7}$$

where $K = \{r \in I\!R^3, ||r_{\mathrm{T}}|| \leqslant \mu r_{\mathrm{N}}\}$ is the usual Coulomb friction cone. Using the modified local relative velocity introduced by De Saxcé and Feng [41, 42], $\widehat{u} := u + \mu \|u_{\mathrm{T}}\| \mathsf{N}$ and the dual cone of K, *i.e.*, $K^* = \{z \in I\!R^3 \mid z^T x \geqslant 0 \text{ for all } x \in K\}$, the contact model is equivalent to

$$K^* \ni \widehat{u} \perp r \in K. \tag{8}$$

3.1.3. Equations of motion with contact and friction

The gap function g_{N} for a contact is generally a function of the configuration of the bodies q. Let us consider that we have a set of m contact pairs given by the unilateral constraints:

$$g_{\mathrm{N}}^\alpha(q) \geqslant 0, \alpha \in \mathcal{I} \subset I\!N, |\mathcal{I}| = m. \tag{9}$$

For a contact $\alpha \in \mathcal{I}$, the relative normal velocity is related to v through the relation

$$u_{\mathrm{N}}^\alpha = \dot{g}_{\mathrm{N}}^\alpha(q) = J_{g_{\mathrm{N}}}^\alpha(q)\dot{q} = J_{g_{\mathrm{N}}}^\alpha(q) T(q) v := G_{\mathrm{N}}^\alpha(q) v, \tag{10}$$

where $J^{\alpha}_{g_{\mathrm{N}}}(q)$ is the Jacobian of g^{α}_{N} with respect to q. The same type of relation can be written for the tangential relative velocity u_{T} as $u_{\mathrm{N}} = G^{\alpha}_{\mathrm{T}}(q)v$ and we get for u^{α}

$$u^{\alpha} \coloneqq G^{\alpha}(q)v. \tag{11}$$

By duality, the total force generated by the contact α is

$$G^{\alpha,\top}(q)r^{\alpha} \coloneqq G^{\alpha,\top}_{\mathrm{N}}(q)r^{\alpha}_{\mathrm{N}} + G^{\alpha,\top}_{\mathrm{T}}(q)r^{\alpha}_{\mathrm{T}}. \tag{12}$$

Altogether the equation of motion with contact and Coulomb friction are given by

$$\left\{\begin{array}{ll} \dot{q} = T(q)v, & \\ M\dot{v} = F(t,q,v) + G^{\top}(q)r, & \\ r^{\alpha} = 0, & \text{if } g^{\alpha}_{\mathrm{N}}(q) > 0, \\ K^{\alpha,*} \ni \widehat{u}^{\alpha} \perp r^{\alpha} \in K^{\alpha}, & \text{if } g^{\alpha}_{\mathrm{N}}(q) = 0, \\ u^{\alpha,+}_{\mathrm{N}} = -e^{\alpha}u^{\alpha,-}_{\mathrm{N}}, & \text{if } g^{\alpha}_{\mathrm{N}}(q) = 0 \text{ and } u^{\alpha,-}_{\mathrm{N}} \leqslant 0 \end{array}\right\} \alpha \in \mathcal{I},$$

3.1.4. Time-discretization

Let us consider a time discretization $t_0 < \ldots < t_{k-1} < t_k < \ldots < T$ with a constant time step $h = t_{k+1} - t_k$. The Moreau–Jean scheme for the system is

$$\left\{\begin{array}{ll} q_{k+1} = q_k + hT(q_{k+\theta})v_{k+\theta} & \\ M(v_{k+1} - v_k) - hF_{k+\theta} = G^{\top}(q_{k+1})P_{k+1}, & \\ P^{\alpha}_{k+1} = 0, & \left.\begin{array}{l}\\ \end{array}\right\} \alpha \notin \mathcal{I}_k \\ K^{\alpha,*} \ni \widehat{u}^{\alpha}_{k+1} + e^{\alpha}u^{\alpha}_{\mathrm{N},k}\mathsf{N} \perp P^{\alpha}_{k+1} \in K^{\alpha} & \left.\begin{array}{l}\\ \end{array}\right\} \alpha \in \mathcal{I}_k. \end{array}\right. \tag{13}$$

where the notation $x_{k+\theta} = (1-\theta)x_k + \theta x_{k+1}$ is used for $\theta \in [0,1]$ and the set $\mathcal{I}_k$ is the set of contact activated at the velocity level

$$\mathcal{I}_k = \{\alpha \in I \mid g^{\alpha}_{\mathrm{N},k} + \gamma u^{\alpha}_{\mathrm{N},k} \leqslant 0\} \text{ with } \gamma \in [0, \frac{1}{2}]. \tag{14}$$

In the time-stepping method, the unknown P_{k+1} is an approximation of the impulses of the contact reaction measure $\mathrm{d}i$ over the time interval, that is

$$\int_{(t_k,t_{k+1}]} \mathrm{d}i \approx P_{k+1}. \tag{15}$$

The contact reaction measure is related to the contact force when the motion is smooth enough by $\mathrm{d}i = r(t)\mathrm{d}t$. The system (Equation 13) is a second order cone complementarity problem that is solved by SICONOS using a Gauss-Seidel method with projection [42].

3.1.5. Comments and remarks on the strengths of the NSCD method

With the NSCD method, robust and efficient simulations ot the dynamics and the quasi-statics of multi-body systems with contact, impact and Coulomb friction are possible. Among them, the scheme integrates the impact equation by consistently approximating percussions. To this aim, the scheme is fully implicit for the unknown P_{k+1} and when the time-step goes to 0, the following impact equations are retrieved

$$M(v_{k+1} - v_k) = G^\top(q_{k+1})P_{k+1}. \tag{16}$$

The non-impulse terms of the dynamics are approximated with a $\theta-$method. For $\theta = 1$, the scheme is fully implicit and maximizes the numerical dissipation. It is therefore well adapted to quasi-static evolutions, or for efficiently reaching a static equilibrium with large time-steps. For $\theta = 1/2$, the mechanical energy (the sum of the kinetic and potential energy) is conserved. Furthermore, the dissipation is always positive and is given by a second order approximation of the actual dissipation. These energy and dissipation properties detailed in [33] render the scheme robust and stable with quite large time–steps, and are of particular interest for the analysis of the dissipative processes in protection structures. These are the main advantages with respect to classical smooth DEM approaches [43, 44] where the use of explicit scheme renders difficult the energy analysis and the contact compliance generates spurious oscillations that prevent to obtain quickly static equilibrium without artificial damping. With a non-smooth dynamics, direct higher order approximations are possible, but some care has to be taken. The use of standard higher scheme — Newmark, HHT, generalised-α, implicit Runge-Kutta to name a few — is not possible and we need to rely on specific schemes such as non-smooth Newmark or generalised-α schemes [45, 46, 47], or time discontinuous Galerkin methods [48, 49].

3.2. NSCD structure model development in SICONOS

By contrast with common applications of NSCD, new challenges raise when modeling such articulated-concrete-blocks structures. These relate to the shape of the concrete blocks, the presence of structural components passing through these blocks, the interaction between these later components and the mod-

eling of the connectors. The model configuration and its components are demonstrated in Figure 5. The modeling strategy that is developed to cope with these specific features is presented hereafter.

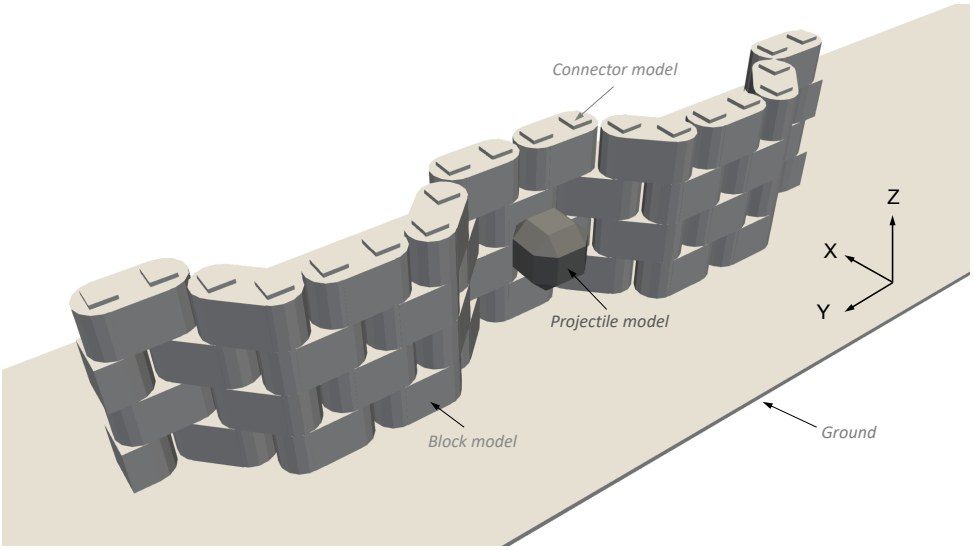

Figure 5: The NSCD model of the articulated concrete block structure and its components

3.2.1. Blocks modeling

In the development of the concrete block model, a particular attention is paid to the block shape and to the mechanical interaction of the block with the connectors. The former issue results from the rounded extremities of the blocks and from the effective contact surfaces between superimposed blocks, as illustrated in Figure 6. The block shape issue thus concerns the interaction between superimposed concrete blocks and the interaction between the projectile and the wall.

The geometry of the blocks was unreasonable to model as a mesh. Replicating the rounded extremities of the block would have induced very large computation times associated with the large number of triangular mesh required for describing their upper and lower faces. It would have also induced computational errors associated with the interaction between superimposed blocks and resulting from contact detection problems. The upper, lower and lateral side faces of the block are thus simplified modeling the concrete blocks as a combination of the so-called primitive shapes which are available in SICONOS.

Different combinations of primitive shapes are considered for geometry and contact area relevance with the experimental block, and for numerical efficiency and computational accuracy in the NSCD framework. This resulted in the best block model option, presented in Figure 7. Several contact points are set along the contact surface to model the interaction between superimposed blocks. The location

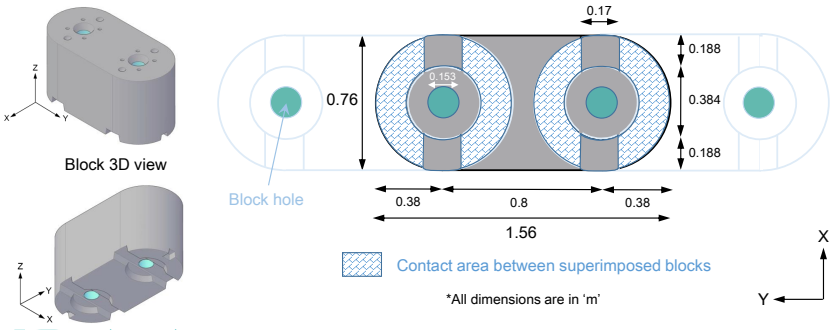

Figure 6: Experimental concrete block design and effective contact surfaces between superimposed blocks

of the contact point is defined in order to maximize the contact surface between the interacting bodies. One can note that, in the case of static equilibrium, the resulting interaction force between the bodies does not depend on the location of the contact forces.

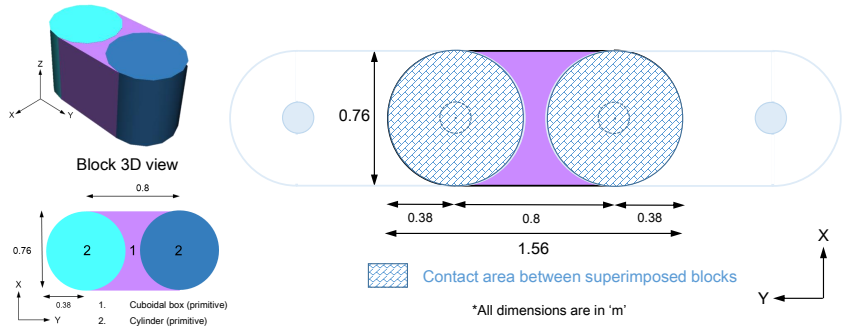

Figure 7: Block design in the NSCD model

Modeling the connectors explicitly as hollow cylinders passing through the blocks would also unnecessarily increase the computation time. These are ignored and a specific strategy is developed for accounting for the interaction between the block and the connectors, as detailed later in section 3.2.4. Besides, the block model has the same mass as of the real block. The inertia of the model blocks is obtained through a 2D surface mesh using the Convex Hull [50] feature in SICONOS.

3.2.2. Connectors modeling

In the real structure, the stacked concrete blocks are connected together via piled up steel tubes through which a steel sling runs from the bottom of the wall to its top (see Figure 1.iv). These connectors were modeled as a single component accounting for the influence on the structure response of both the sling and tubes. It required defining a mechanical model governing the connector- block interaction (which is insured by the tubes) and the interaction between connectors (which is in particular controlled by the slings). The collective connector model illustrative profile is presented in Figure 8 for before and

after impact situations.

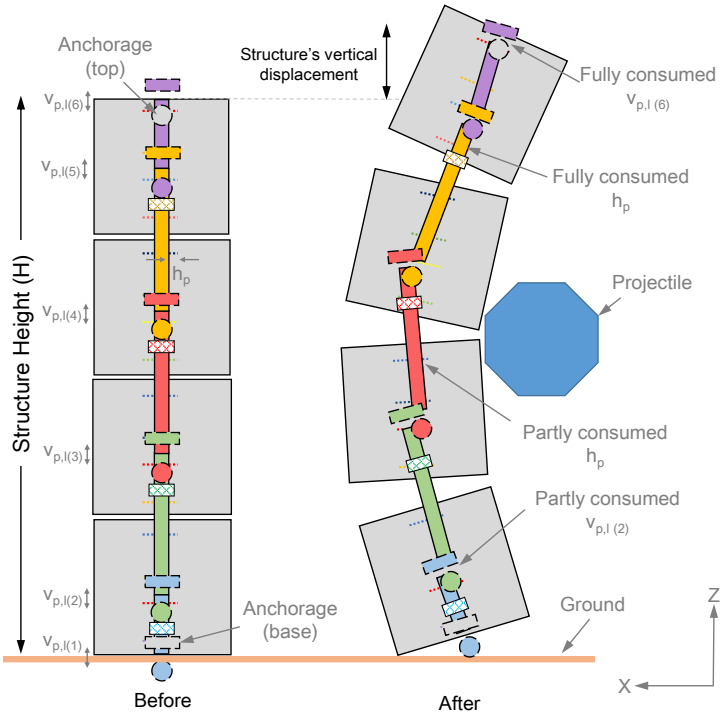

Figure 8: Schematic representation of the deformation of the structure upon projectile impact showing plays in action

It consists in five cylindrical primitive shape components, named as bars, at location corresponding to the real-structure tube positions and possessing same length (3 bars with 0.8m and 1 bar with 0.4m), diameter, inertia and mass as the tube. Notably, a fifth bar is added at the top block having similar geometrical characteristics as of the short length bar, however with a negligible mass. This is done to complete the configuration and the bounding limits of the sling in the real structure.

The mechanical plays existing in the structure, in both the horizontal and vertical directions are accounted for in the model. The horizontal play in the real structure results from the difference between the external diameter of the tube (139.7mm) and the diameter of the hollow cylinder in the block (154mm). In the model, the horizontal play (h_p) is rounded to 7mm (Figure 9). The vertical play in the real structure results from the relative looseness in the sling. The detailed connector modeling strategy to accommodate horizontal and vertical plays is presented hereafter.

In the model, the connectors pass through the concrete blocks but there is no direct interaction between them. This interaction is assigned through hollow circular disks added to the block model object, as illustrated in Figure 9. These disks are modeled as 2D mesh and have same internal diameter as that of the hole in the real block, hence ensuring the presence of the requisite horizontal play. Each

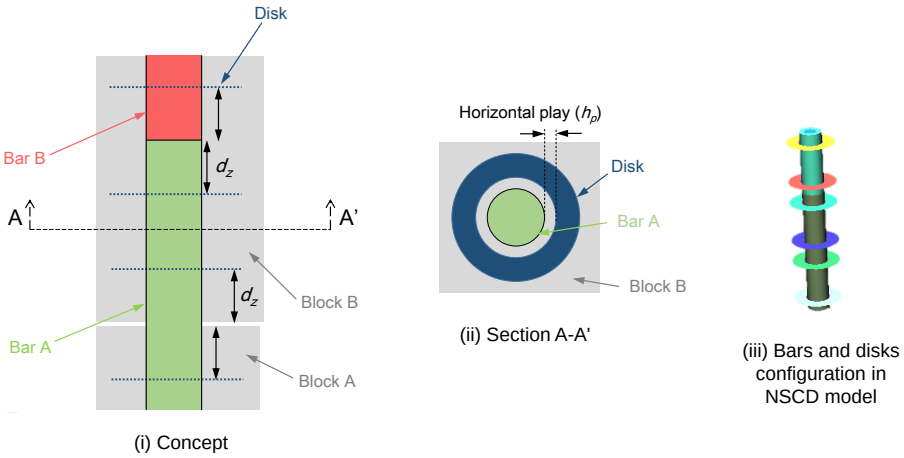

Figure 9: Concept of the connector modeling incorporating horizontal play

block is equipped with four hollow disks meaning that each of the two bars passing through a block interacts with this block via two disks. The position of these disks with respect to the lower/upper block faces and to the bars extremities is characterized by parameter d_z, which is kept alike for simplicity. The positioning of these disks can not be explicitly defined and hence it is characterized as a model parameter.

The vertical play is considered equally distributed along the structure's height as six local vertical plays ($v_{p,l} = v_p/6$) whose development is described as follows. Bar objects are assigned as invisible to each other and are equipped with three additional components accounting for the influence of the sling, presented in Figure 10.

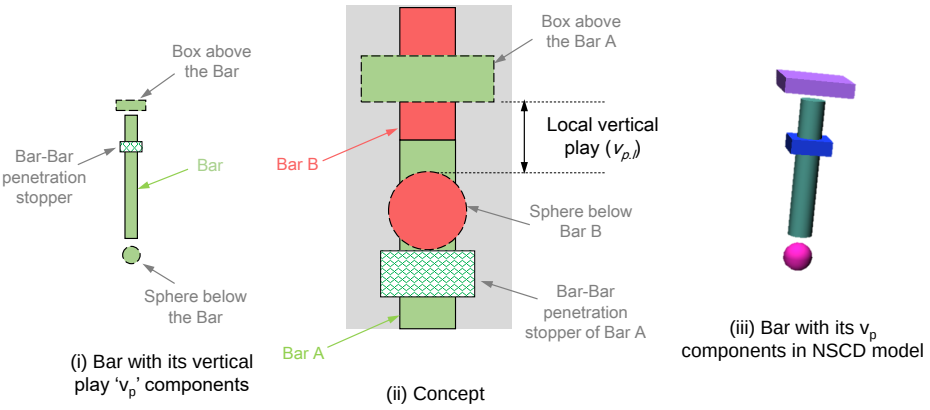

Figure 10: Concept of the connector modeling incorporating vertical play

These components are comprised of a cuboid box of length equal to 2.5 times the bar diameter (placed above the bar), a sphere of diameter equal to the bar diameter (placed below the bar and another cuboid

box of length equal to 1.5 times the bar diameter (placed within the bar) named as 'bar-bar penetration stopper'. The vertical position of these components are assigned such that the sphere from the adjacent bar detects the contact with the boxes of the current bar. The distance between the box placed above the bar and the bar surface, as well as the distance between the sphere and the bar surface, is half the local vertical play. This way, the box-sphere combination from two adjacent bars collectively accounts for the local vertical play. The bars interpenetration is avoided via the contact detection between this bar-bar penetration stopper and the sphere from the adjacent bar.

All components of each block (and also bar) model objects have no relative movement between them. This feature enables to indirectly implement the block-bar interaction and sling functionality representative of the real structure. An illustrative representation of the connector model (inclusive of the plays) in action is added in Figure 8 for understanding. Here, the interaction of the vertical play constituents (box and sphere) can be clearly seen. The distribution of vertical play (as six local vertical plays) enables to mimic the looseness in the sling as an indirect chain made from multiple linkages. Once the complete vertical play is consumed, the setup of bars mimic the tension in the sling. Such a state is reached depending (mostly) on the assigned looseness in the vertical play and the energy of the impacting projectile. This makes the vertical play (v_p) as a model parameter.

This intricate setup allows to model the large displacements in the model structure courtesy to the accompanying horizontal play (h_p). Its presence controls the maximum relative lateral displacement between box and sphere components of the vertical play. Thereby, a possible contact between the vertical play components from adjacent bars is always ensured, which makes the connector model's functionality robust. An additional box and a sphere are added at the bottom and top most layer of blocks respectively. This is to respectively mimic the anchorage of the sling with the structure's bottom and to make sure the bars do not fly-out of the structure's top surface upon impact.

3.2.3. Projectile modeling

The experimental equivalent projectile is modeled as a convex 2D mesh of manually assigned vertices. The projectile shape and size ($1/3^{rd}$ of the wall height) features are in accordance with the requirements for flexible barriers testing [51]). The mass of the projectile is assigned 2600 kg, and the inertia is assigned through convex hull (as used for block model). The input kinetic energy corresponding to the two impact tests (*i.e.,* 520kJ and 1020kJ) is derived to assign the input velocity to the projectile model.

3.2.4. Interaction laws

The model objects (*i.e.,* blocks, bars, projectile and ground) are defined as a combination of different components called contactors, collectively making the model equivalent to the real structure. These contactors are defined with a uniquely assigned collision group to identify them and differentiate one from another. The collision groups of the contactors in the model bodies are listed in Table 2.

Table 2: Model bodies constitution for interaction

Collision group	Contactor	Collision group	Contactor
0	Block (cuboid portion)	5	Hollow disk
1	Block (curvature portion)	6	Box (vertical play)
2	Bar (odd)	7	Sphere (vertical play)
3	Bar (even)	8	Projectile
4	Bar-Bar penetration stopper	9	Ground

The interaction between model bodies is assigned through Newton impact friction non-smooth law [3]. This law governs the interaction between a pair of contactors (identified through their respective collision groups) via user-defined coefficient of friction (μ) and coefficient of restitution (e). The assigned interaction laws in our NSCD model are listed in Table 3. Here, the various interactions in the numerical model bodies are chronologically listed, analogous to the construction of real structure.

The interaction along the tangential direction between the projectile and the blocks and that between blocks are governed by the concrete-concrete friction coefficient (μ_{cc}). Similarly, the interaction of each block of the wall with the ground is governed by the concrete-soil friction coefficient (μ_{cs}). The restitution coefficient (e) is kept the same for both of these interaction types.

Besides, all interactions between steel material and blocks and ground are assigned a constant friction coefficient of a relatively low magnitude of 0.2 for a minimum energy dissipation through these frictional interactions in the overall model system. Also, the restitution coefficient with magnitude 0 is assigned presuming all such contacts being perfectly inelastic (*i.e.,* no rebound after contact). Moreover, as the sling is a continuous element and bars do not interact with each other, the friction coefficient between the boxes and sphere of connector elements (vertical play and penetration stopper) is assigned zero. This is

Table 3: Assigning the interaction between model bodies contactors

Construction	Interacting pair (Colliding groups)	Friction	Restitution
Foundation	Block (1) - Ground (9)	μ_{cs}	e
	Cylinder (2) - Ground (9)	0.2	0
Stacking blocks	Block (1) - Block (1)	μ_{cc}	e
Inserting tubes	Odd bar (2) - Disk (5)	0.2	0
	Even bar (3) - Disk (5)	0.2	0
Inserting sling	Box (6) - Sphere (7)	0	0
	Penetration stopper (4) - Sphere (7)	0	0
Impacting the wall	Block (0,1) - Projectile (8)	μ_{cc}	e

to indirectly represent consistent stretching in the sling as local vertical plays starts to be fully consumed and subsequently tension in the sling in the event of complete consumption of the available vertical play. Also $e = 0$ in the bar to disk contact assures no relative rebound once the horizontal play is consumed and the bar comes in contact with disk (analogues to tube and concrete block hole interaction in the real structure.)

3.3. Simulation database

The structure model is impacted at the wall center height and in the middle of its footprint length. A demonstrative post impact deformed structural conformation is presented in Figure 11. Here, the initial (pre-impact) configuration is also presented (similar to Figure 5) where transparent blocks reveal the underlying connector model characteristics.

The HDF5 output file of the model impact test provided the detailed information on the displacement, rotation and velocities of each block and thereby enabled a direct comparison with the experimentally obtained results at the corresponding locations. Besides, a detailed output database recorded for the contact forces also enabled the additional post-processing of the model structure behavior extending the limits of the experimentally acquired database to a computationally advanced level.

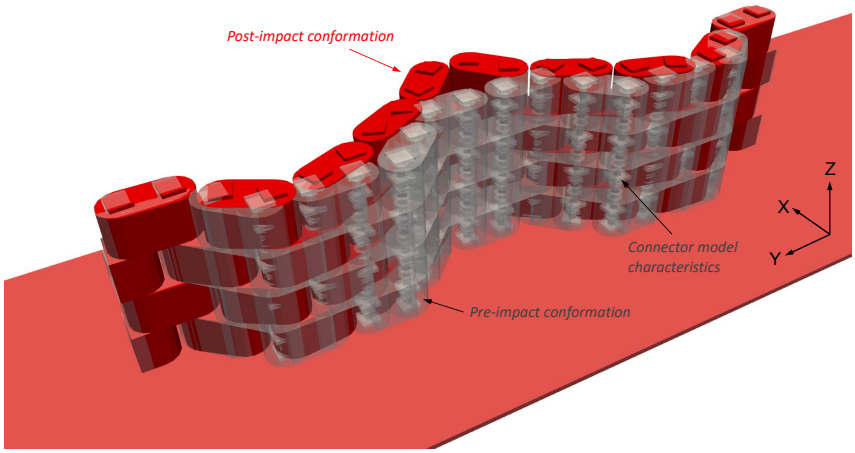

Figure 11: Qualitative representation of initial and post-impact model conformations and highlighted connector model characteristics

3.4. Evaluation of the NSCD model response

The presented NSCD model comprises of many input parameters, most of which are directly taken from the real structure description (Table 1). By contrast, five model parameters couldn't be given a precise value from this description. The first two take into account the imposed constraints for the block-connector (d_z) and connector-connector (v_p) interaction while the other three concern the interaction laws between contacting bodies (μ_{cc}, μ_{cs} and e).

The relative disk position (d_z) could not be precisely derived from the block and tube geometry. The vertical play (v_p) magnitude is variable from place to place in the structure and it is difficult to measure precisely. The coefficients governing friction between blocks (μ_{cc}) and that between the blocks and the soil (μ_{cs}) are difficult to measure precisely as dealing with the dynamic loading of an articulated structure where relative movement between bodies include translation and rotation. Last, the restitution coefficient (e) is a model parameter whose precise value couldn't be derived from some mechanical or geometrical features of the real structure.

These parameters are listed in Table 4 with their range of possible values. The range for the vertical play is derived from observations on the real structure. The range for the disk position is determined as fraction of the block height. The concrete-concrete friction angle is considered with the applicable range information retrieved from the literature [52]. The range for the friction angle between concrete and soil is established assuming slightly higher values than between concrete and concrete. The restitution coefficient magnitude is considered ranging from perfectly inelastic collision (*i.e.*, $e = 0$) upto a magnitude

Table 4: Model parameters with their considered range and mean value

Parameter	Possible range	Mean value	Unit
Bar-block contactor disk position (d_z)	5 - 10	7.5	cm
Vertical play (v_p)	1 - 10	5.5	cm
Friction coefficient concrete-concrete (μ_{cc})	0.25 - 0.55	0.4	(-)
Friction coefficient concrete-soil (μ_{cs})	0.3 - 0.6	0.45	(-)
Restitution coefficient (e)	0 - 0.3	0.15	(-)

364 towards perfectly elastic collision. This upper limit is selected based on multiple simulations such that
365 the rebound effect does not cause excessive inter-blocks displacement.

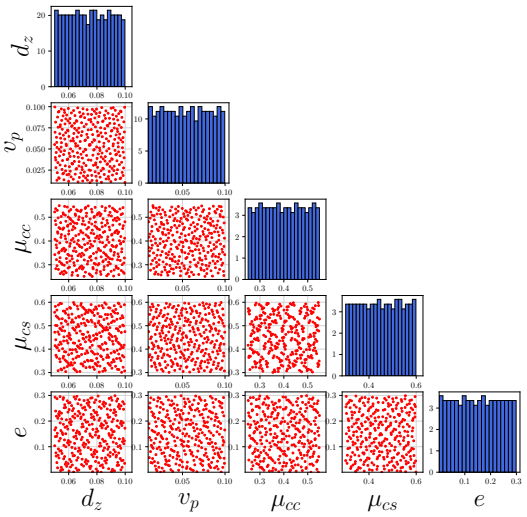

Figure 12: Input sample of size 300 (based on Sobol' sampling method) comprising of five parameters following uniform distribution in their respective ranges of variability

366 As a first step, the overall response of the NSCD model is assessed through a sample set of different
367 combinations of the five input parameters. This sample set is statistically generated using sampling
368 methods based on MC and quasi MC (such as Sobol', Halton) [53] implemented in the UQlab input
369 module [54]. The Sobol' sampling method is used to define a set of 300 combinations of these five input
370 parameters, as presented in Figure 12. This sampling method provides a random selection of the input
371 parameters within their predefined ranges such that the input space is well-filled. Besides, without any

prior bias to the magnitude of the five model parameters, uniform distribution are assigned for all.

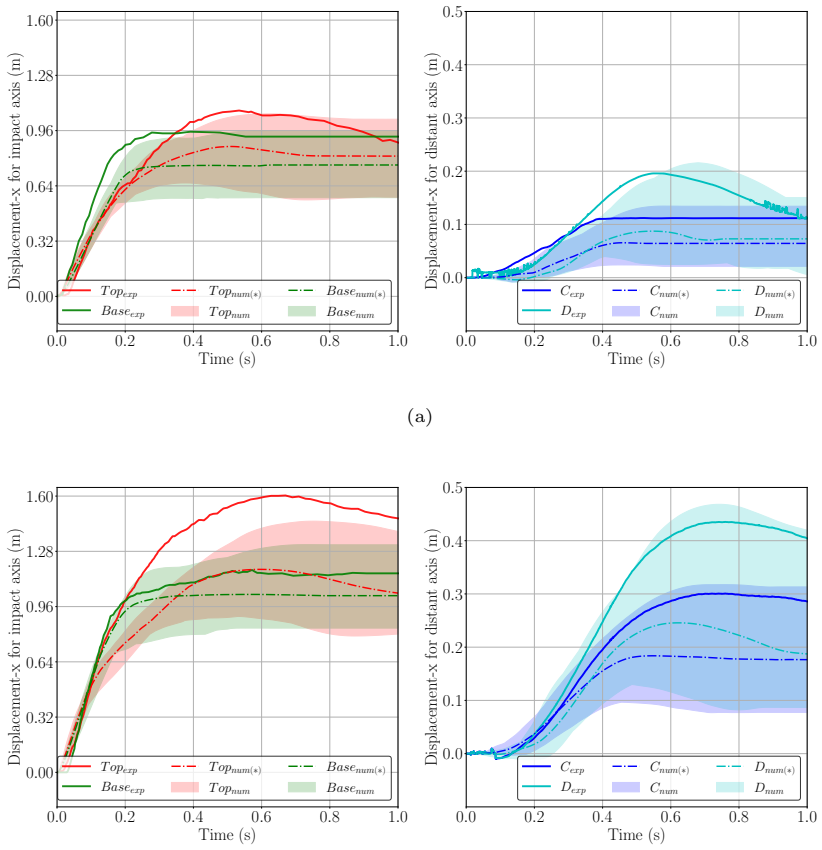

(a)

(b)

Figure 13: Comparison of the experimental observations against the range of numerical computation response for displacement for (a) 520kJ and (b) 1020 kJ impact energy tests. The response obtained from the deterministic set of mean values of model parameters is also highlighted.

The global minimum and maximum range of outcomes from these 300 different simulations is presented in Figures 13a and 13b together with the NSCD model outcome from the mean value set of the input parameters. Globally, the range of numerical outcomes envelops the experimental observations at all measurement points. However, the range of model outcomes for the 'Top point' remain below the experimental observations for the 1020 kJ impact. In this case, concrete blocks in the impact vicinity experienced severe damage, up to fracture, resulting in a decrease in the mechanical continuity within the structure, which was thought to result in a higher blocks displacement at the wall top. This introduced a difference between the real structure and its numerical counterpart where no concrete block fracture is possible.

In spite of this difference, the overall model to experiment correspondence is good considering all the

data describing the structure response. This suggests that the NSCD model has the capacity to model the structure global response. Also, the envelop infers that there could exists at least one set of five parameters that allows the NSCD model to possibly replicate the experimental response. This demands an extensive model calibration procedure presented hereafter.

4. Calibration of the NSCD model

The five parameters presented in Table 4 are calibrated so that the simulated spatio-temporal structure impact response mimics that of the real structure considering four observation points (*i.e.,* points Top, Base, C and D as shown in Fig. 2). The time evolution of the displacement along the x-axis is accounted for considering three representative time instants. As classically done, the displacement at rest and the maximum displacement are considered. In the following, these are referred to as *rest* and *max* respectively. The third time instant focused on the initial stage where the displacement is fast and varies rather linearly. The corresponding time instant is arbitrarily fixed to 0.1 after the impact beginning in the impact axis (*i.e.,* for points Top and Base) and 0.25 s in the distant plane (*i.e.,* for points C and D). This third displacement value, hereafter referred to as *init*, aimed at reflecting the dynamics of the structure. The displacement measured at these three time instants are considered to present a global narrative of the structure's displacement, and thus performance in the point of view of its practical application.

4.1. Calibration strategy

The five model parameters are calibrated considering the displacement at the four measuring points, at the three different times and for the two impact experiments. The calibration is performed using the Bayesian interface statistical learning procedure on the meta-model of the articulated model structure, following the conceptual pathway presented in Figure 14.

This complex pathway is motivated by the fact that reaching this ambitious calibration objective demands a very large number of model computations. This is practically impossible with each model computation taking up to 20-30 minutes. This limitation is averted using surrogate models of the structure response for different points at various time instances. The surrogate model development and subsequent model calibration is presented hereafter.

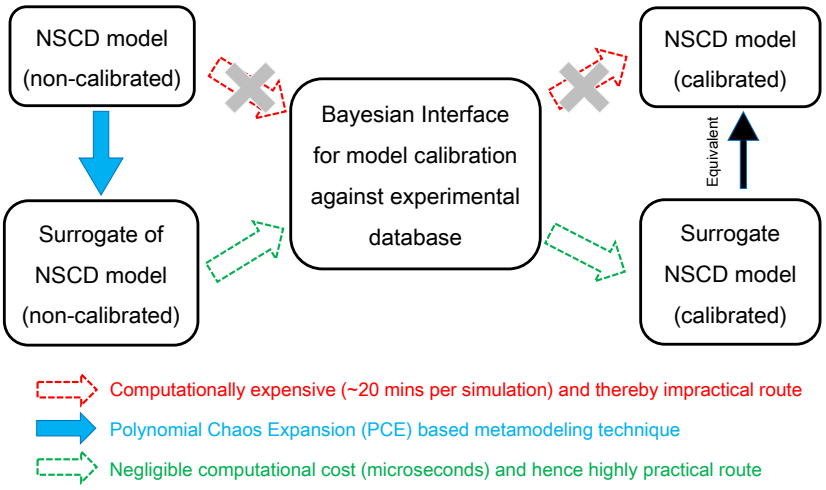

Figure 14: Conceptual work flow of the NSCD model calibration using a combination of stochastic methods

4.2. Meta-model creation and accuracy assessment

A meta-model is a mathematical modeling tool which bridges the gap between the current version of the numerical model and the requisite large number of computations for stochastic analysis. Here, the small statistically created input sample of the model parameters (presented in Figure 12) is used to define the mathematical expression incorporating the model behavior with the desired accuracy. A polynomial chaos expansion (PCE) based meta-modeling technique is used to create the surrogate of the NSCD model in the framework of UQ[py]Lab (a python library of UQLab [55]). Here, the set of results from the 300 NSCD simulations is considered for the meta-model creation following the method described in Appendix A. The resulting mathematical expression (*i.e.,* meta-model) can be analogically referred to as obtaining a regression for a 2D database.

The PCE based meta-models are built upon the displacement response at three time instances-at four different points-for two different energies, thereby, summing to a total of 24 meta models. The accuracy assessment revealed a leave-one-out (LOO) error (Equation A.5) in the order of 10^{-2} to 10^{-1} for all the computational cases. Thereby, as the NSCD model is highly nonlinear and non-smooth, we accept the meta-model accuracy and the underlying uncertainty. Such level of accuracy is deemed sufficient for the upcoming Bayesian interface based calibration method with the advantage of a single model computation within micro-seconds.

Further, the accuracy of the meta-models is assessed by comparing the meta-models predictions with the NSCD model computations for the 520 kJ and 1020 kJ impact tests (Figures 15a and 15b). Notably,

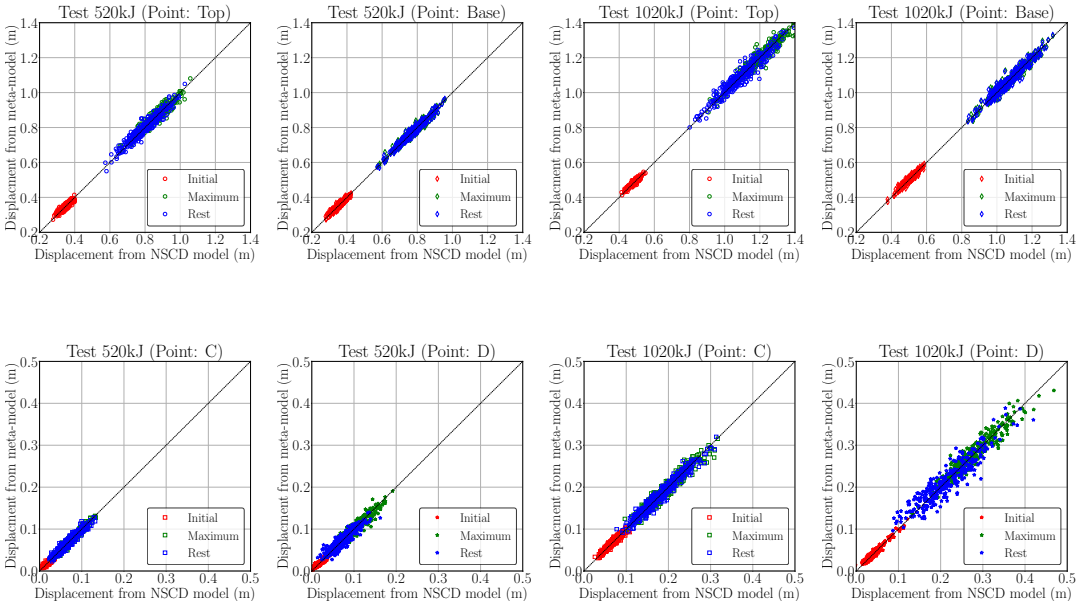

Figure 15: PCE based meta-model validation at three different locations for (a) 520kJ and (b) 1020 kJ impact tests

the set of 300 NSCD model simulations that was used to create the meta-model is reused as a validation. The choice of not using an independent set is made based on the order of magnitude of LOO and the relative difference between NSCD and meta-model outputs for the same set of input parameters.

The cloud of points are rather well aligned with the diagonals in these plots, indicating that the predicted response by the meta-models fits with the corresponding NSCD simulations results. The reliability of the predictions along the impact axis is relatively better than in the distant one for both impacts. The distant axis points move relatively less and presents more divergence from the diagonal line. It highlights the significance of the variability in model dynamics farther from the impact axis as the model interaction parameters vary.

4.3. Relative influence of the model parameters

Before proceeding with the calibration process, the influence of each parameter on the spatio-temporal displacement response of the structure is investigated through the Sobol sensitivity method also known as analysis of variance (ANOVA) [56]. This method decomposes the variance of the output parameters as the sum of the contributions of the different input parameters including the possible interaction between input parameter. Each contribution is characterized by the ratios of the partial variance to the total

variance, called Sobol sensitivity indices. In this study, we used the total Sobol indices to quantify the total effect of a given input parameter including all possible interactions.

The accurate Sobol indices computation demands a large number of model computation (of order 10^6). This is highly impractical in the present study if the NSCD model is to be used directly. Nonetheless, the meta-model of the NSCD model can be directly used to compute Sobol indices at zero cost [57, 58]. The UQlab sensitivity analysis module [59] is used for such computations. The total Sobol indices for the three time instances, at all considered points and for both impact tests are presented in Figure 16.

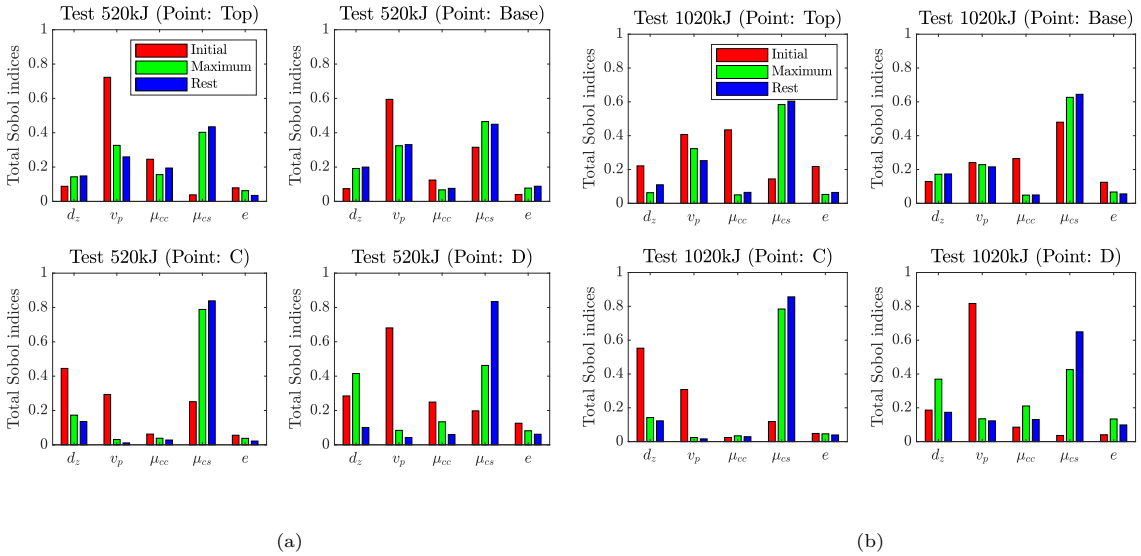

Figure 16: Total Sobol indices of the spatio-temporal displacement response for the sensitivity analysis of the NSCD model parameters for (a) 520kJ and (b) 1020kJ impact test

Overall, these results aid in understanding the structure response highlighting the mechanisms at work with time, complimenting the discussion in [27]. The Sobol indices are observed significantly differ from one parameter to the other. The higher values are observed for the vertical play (v_p) and concrete-to-soil friction coefficient (μ_{cs}). For example, the Sobol index of v_p exceeds 0.7 for the initial displacement at point D, for both impact energies. Also, the Sobol index of μ_{cs} exceeds 0.8 for the displacement at rest at point C, for both impact energies. Even though other parameters globally exhibit lower Sobol indices, none is negligible.

For example, the restitution coefficient (e) globally exhibit the lower Sobol indices, but a value higher than 0.2 is obtained for the initial displacement at the top for the 1020kJ impact. Figure 16 also reveals that the values of Sobol indices for a given parameter vary over time and differ from one impact energy to the other. The Sobol indices of v_p exceeded 0.7 considering the initial displacement at the top for the

the 520kJ impact, while it is close to zero considering the displacement at rest at point C for the 1020-kJ impact. Similar observations are made on the influence of other parameters, as for example comparing the Sobol index of e for the maximal displacement at point C during the 520kJ impact (0.04) to that for the initial displacement at the top during the 1020kJ impact (0.22). The non-zero Sobol indices for each parameter at all computed time instances validates the identifiability of all parameters [60] for upcoming Bayesian interface based studies.

Besides, the sum of indices for a given situation exceeds one (in some cases) which expresses the interaction between input parameters, *i.e.,* the influence of some parameters being dependent on the value of some other parameters. The influence of the vertical play, v_p, on the displacement of the upper blocks during both impact tests decreased with time, from the so-called initial stage to the position at rest. This highlighted that the significant upward displacement (*i.e.,* positive z-axis) of the blocks initiated in the early stage after the impact beginning. By contrast, the influence of the concrete-to-soil friction coefficient, μ_{cs}, showed a global increasing trend with time, which is attributed to the progressive base sliding of the wall. Furthermore, the Sobol index of the concrete-to-concrete friction coefficient, μ_{cc} suggested that the relative displacement between blocks, is much higher in the upper part of the structure (Top and Point D). Overall, non-zero magnitude of all parameters affirms to consider their variability for calibrating the structure response presented hereafter.

4.4. Bayesian interface for model calibration

The Bayesian process for model calibration is inspired from the Bayes' theorem [61] which is simply a representation of the changing beliefs. In simple words, it demonstrates that probability of a hypothesis being correct becomes more reliable when supported with the concerning evidences. In the context of the present work, our hypothesis is that the 300 sets of possible input parameters give a range of displacement values output that is correct. In addition, the experimental observations data is the evidence recorded. Now, the idea of increasing the reliability on our hypothesis given the evidence would be to say that there exist at least one set of input parameters such that the recorded evidence is reproduced and hence, in other words, the model is calibrated. In the context of model calibration, the goal is to find the optimal values of the input parameters that allow one to best fit the model predictions to the observations. A brief description of the Bayesian's interface is presented in Appendix B.

4.4.1. Representation

The available displacement experimental data at the points of interest and at three time instances are taken as a benchmark to calibrate the NSCD model parameters to obtain the requisite set of parameters. The Bayesian interface, similar to a typical stochastic analysis method, demands a large number of model computations for its reliable functionality. In the present work, such essential requirement poses computational time constraint as each NSCD model computational run lasts for about 20 minutes.

This point motivated the use of PCE based meta-models of NSCD model, presented above, to accelerate Bayesian computations, an approach extensively used by many researchers [62, 63, 64]. Here, these meta-models serve as a forward model (or prior) which are created through an extended version (*i.e.,* larger sample size) of the input sample presented in Figure 12, thanks to the surrogate NSCD models. The meta-model based calibrated set of input parameters (*i.e.,* posterior) is thereby a representative of the NSCD model calibration.

The discrepancy (see Equation B.5) of order 10^{-20} is manually assigned. This choice is made with an underlying hypothesis that the experimental measurements are very precise and we wish to retrieve the model input parameters which result in the corresponding measurements. Notably, this value influences the calibration process and thereby in further study its magnitude should be carefully chosen so as to represent the true model and the observation error.

4.4.2. Implementation

The Bayesian interface is implemented to obtain a set of input parameters considering three approaches referred to as 'point', 'energy' and 'all'. These three approaches are inspired from the scope of user's interest to reproduce the experimental outcome which ranges from a particular time instance calibration to overall model behavior calibration in both space and time. The first approach amounts to giving priority for a given point in the calibration process, meaning that the model is calibrated to provide precise predictions over time for this specific point. The second approach, 'energy' is in line with strategies consisting in calibrating a model at a given impact energy before using it for an other impact energy. By contrast with the two previous ones, the 'all' approach aims at ensuring that the model provides reliable predictions at any point and whatever the impact energy. Bayesian interface module in UQLab [65] is used to implement all three calibration approaches.

The calibrated sets of input parameters are reported in Table 5 obtained as a maximum a posteriori

Table 5: Calibrated sets of model parameters following three different approaches

Parameter	Approaches											Units
	Point								Energy		All	
	520kJ				1020kJ				520kJ	1020kJ		
	Top	Base	C	D	Top	Base	C	D				
d_z	5.7	9.6	5.3	5.4	9.5	6.2	6.8	5.0	7.2	6.8	6.8	cm
v_p	5.2	3.8	6.7	6.5	9.0	8.0	7.6	7.0	6.5	7.1	7.1	cm
μ_{cc}	0.251	0.419	0.474	0.265	0.378	0.512	0.510	0.342	0.351	0.323	0.316	(-)
μ_{cs}	0.311	0.304	0.340	0.346	0.306	0.351	0.301	0.301	0.320	0.308	0.307	(-)
e	0.190	0.194	0.138	0.033	0.152	0.290	0.283	0.200	0.198	0.220	0.222	(-)

(MAP) and mean point estimates (see Equation B.15) for 'point' approach and for both other approaches respectively. Depending on calibration approach, significant differences in parameter values are observed. For example, v_p varied from 3.8 to 9 cm depending on the calibration strategy. A ratio of about two between the minimum and the maximum values attributed to a parameter is also observed for d_z and e in particular. Interestingly, the set of values calibrated following the 'all' approach is very close to that obtained following the 'energy' approach while considering the 1020kJ impact.

4.4.3. Interpretation

The displacement response comparison between experimental results and NSCD model results obtained considering the magnitude of these input parameters is presented in Figure 17. The interpretation on these observations is presented hereafter.

The first approach (*i.e.,* 'point' approach) results in a total of four calibrated set of input parameters for each impact test. This approach allows to represent the influence of model dynamics at different points as the best set of input parameters is reported distinct for each point and for both energies. The experimental and numerical response, respectively in *black* and *red* in Figure 17, are in a very good quantitative and qualitative agreement with each other justifying the usage of stochastic methods for model calibration. This very good agreement emphasizes the success of choosing only three representative time instances over the whole impact duration. The significant difference observed at top point for

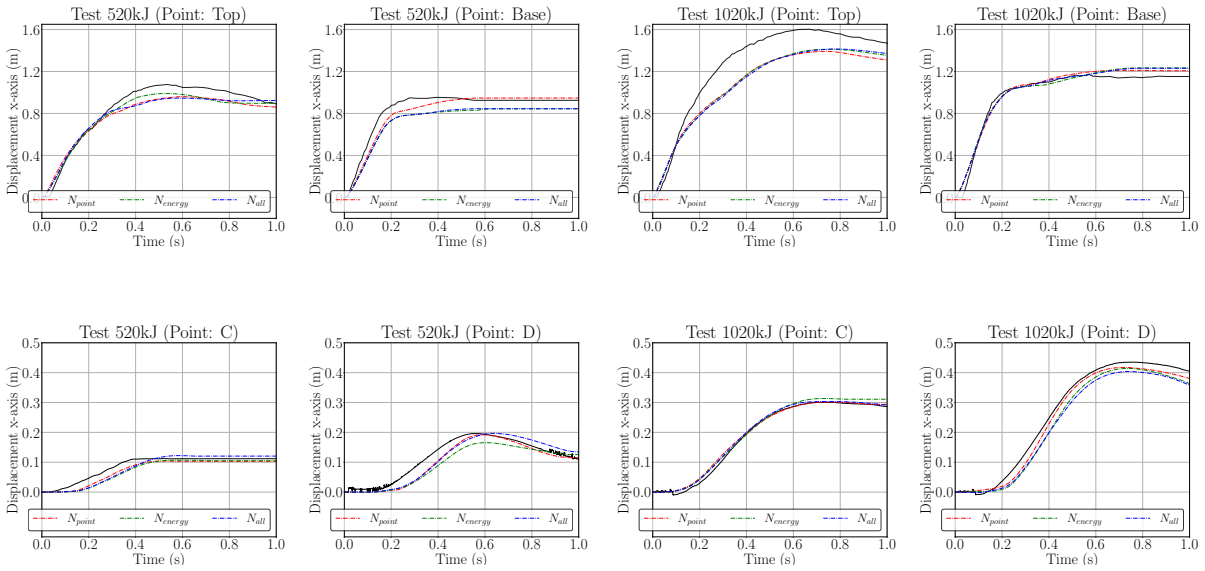

(a) (b)

Figure 17: Bayesian inversion based calibration of (a) 520kJ and (b) 1020kJ impact test. Curves in *black* show the experimental data. Curves in *red*, *green* and *blue* show the NSCD simulation results corresponding to approaches 'point', 'energy' and 'all', respectively.

1020kJ test is attributed to the loss of mechanical continuity as discussed in section 3.4. The obtained eight distinct sets of parameters (Table 5) highlight the significance of local dependency of the model constitution to accurately replicate the experimental response.

The second approach (*i.e.,* 'energy') collectively takes into account the model outputs at three time instances for all four measurement points for a given impact test. This way, two calibrated sets of input parameters are obtained from the Bayesian interface one each for 520kJ and 1020kJ impact test. This approach presents the influence of the impact energy on the global model response. The corresponding response obtained from the NSCD model run (*in green*) is compared against the experimental observation. Similar to the 'point' approach, a good qualitative agreement is observed between the experimental and numerical responses. Courtesy to the multi-model calibration possibility (through group Likelihood computation, see Equation B.10) in Bayesian interface of UQlab [65], the recorded 'energy' response using a single set of input parameters presented a similar response to the four distinct sets of these parameters in 'point' approach for each energy level.

The third approach (*i.e.,* 'all') collectively takes into account the model outputs at three time instances for all four measurement points for both impact tests. Hence, a single set of calibrated input parameters

is obtained representing the global response of the NSCD model, with time and space. Here again, the comparison between the corresponding response obtained from the NSCD model (*in blue*) is in good qualitative and quantitative agreement with the experimental observation.

4.4.4. Application

Finally, the counterpart of the input sample distribution before the calibration (see Figure 12, the posterior input sample distribution obtained from the 'all' approach is presented in Figure 18. The data-point corresponding to the calibrated set - here and in different locations in the text is also highlighted. Notably, from the histogram of the outputs, all input parameters present a locally emphasized magnitudes corresponding to the good fits with the desired output. However, the final set of parameters deviates slightly from the most probable magnitude of a particular input parameter. This difference is negligible for all parameters except μ_{cc} where the final selected parameters magnitude is slightly larger than the most probable one. Besides, a very narrow range of μ_{cs} parameter indirectly highlights its relatively high sensitivity to the model response (as also highlighted in Figure 16).

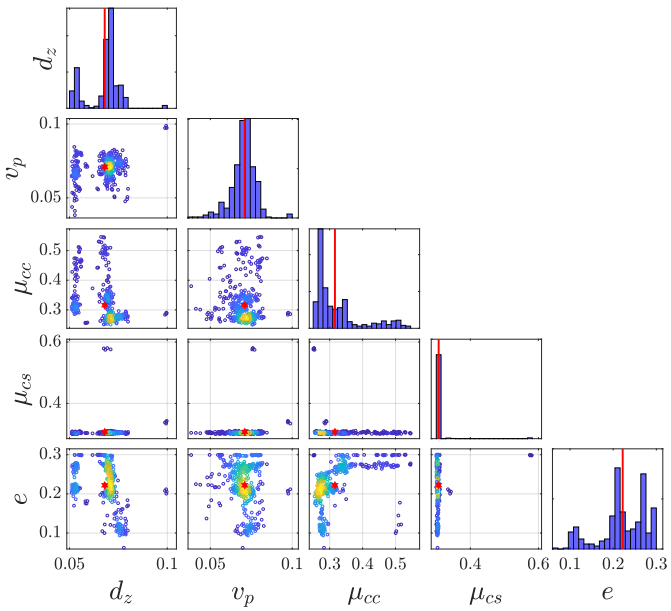

Figure 18: Posterior sample distribution of five model parameters obtained from Bayesian interface application as per 'all' approach. The mean point estimate (in red) highlights the calibrated values of the respective model parameters

Further, as the counterpart of the displacement response before the calibration process (see Figure 13), the post-calibration response (from 'all' approach) is presented in Figure 19. Overall, a good qualitative agreement between experimental and numerical observations is reported favoring the calibrated set of

input parameters. From the quantitative comparison of the collective experimental and numerical (posterior mean) displacement measurements at three time representative, a root mean square error (RMSE) of 9.9cm and 2.3cm is reported for impact and distant axis respectively which account for about 8.6% and 5.6% of representative displacements from the respective axis. A relatively better accuracy to reproduce the distant axis response favors the model practical utility. Continuing with the loss of mechanical continuity argument for the top point during the 1020-kJ test, the reported relatively large quantitative and qualitative difference is accepted and also is not considered in RMSE estimation.

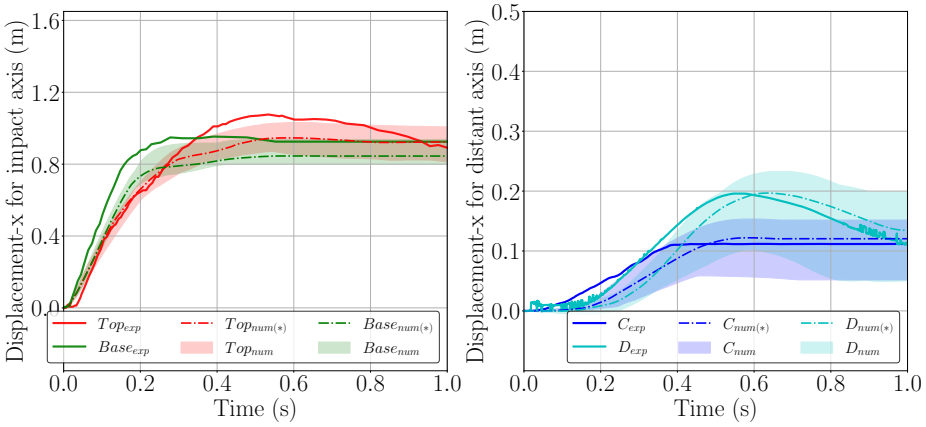

(a) posterior for 520kJ

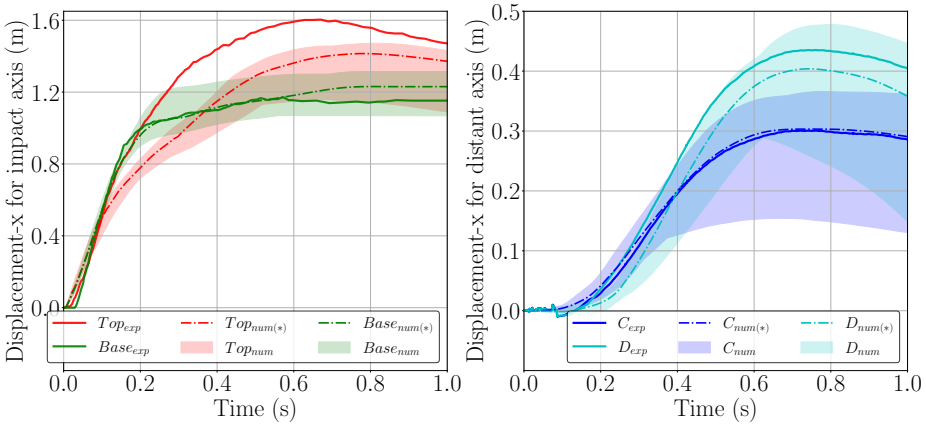

(b) posterior for 1020kJ

Figure 19: Comparison of the experimental displacement response against the NSCD model response obtained from the best calibrated set of input parameters along with the band of possible posterior sample based outcomes for (a) 520kJ and (b) 1020kJ impact tests respectively

Moreover, the range of possible model outputs is also presented using all set of input parameters from the posterior distribution. The relatively narrow width of the band in comparison to the prior sample

validates the computational efficiency of the Bayesian interface. Besides, in co-relation to the input sample distribution, most of the output trends in the band are likely to be closer to the posterior-mean response. Nonetheless, such co-relation is not made as the eventual goal is to obtain a deterministic set of input parameters for further utility of NSCD model.

Globally, the NSCD model is well-calibrated as a positive consequence of the Bayesian interface approach where a large number of model computations are favored by the usage of the PCE based meta-models. As an extension, for a better and more reliable model calibration, the diversity in the experimental data both in time and space is favorable.

5. Discussion

5.1. On the calibration strategy

The results presented in section 4.4 revealed that very different sets of model parameters may result in similar responses over time at a given point in the structure. This is evidenced comparing the NSCD model results when calibrated following the 'point' approach to that following the 'all' approach. The coherent response obtained through the presented three approaches also expresses the advantage of not prioritizing the response recorded at a particular point (using 'point' approach) to represent the overall model behavior. This is because of the large variability in the reported input parameters at different points where a particular set corresponding to a particular point (if prioritized) may not necessarily provide a good response at other point and by extension at a different energy level.

In addition, these results also revealed that the parameter values for a calibrated model are extremely dependent on the calibration strategy. Ratios of about two are observed between extreme values of a given model parameter from one strategy to the other. This is consistent with the idea that the intended use of the model should be taken into account when calibrating the model. Indeed, a calibration based on the displacement with time at a single point in the structure will result in a set of model best fit parameters that may not be reliable for estimating the structure response at another location.

Overall, a relatively low quantitative difference in the displacement output responses between all three approaches is observed, demonstrating that calibrating the model considering a large number of data is not at the expense of a reduction in prediction capacity as compared to models calibrated for a more specific purpose. In other words, the agreement with the experimental data at a given point of a model

calibrated according to the 'all' approach is nearly similar to that obtained with the model calibrated for each specific point, following the 'point' approach.

To demonstrate this, the limitation of 'point' calibration approach to correctly represent spatial-temporal displacement response is demonstrated in Figure 20. Here, the calibration set corresponding to the point Base of 520kJ impact test is presumed representative of the whole structure's response. It is clearly seen that, despite a very good qualitative and quantitative agreement with the experimental response at it's own identity, it fails to correctly reproduce the responses at nearly all remaining locations for 520kJ test and by extension to all four locations of the 1020kJ energy test. Hence, the significance of using all spatio-temporal database is justified.

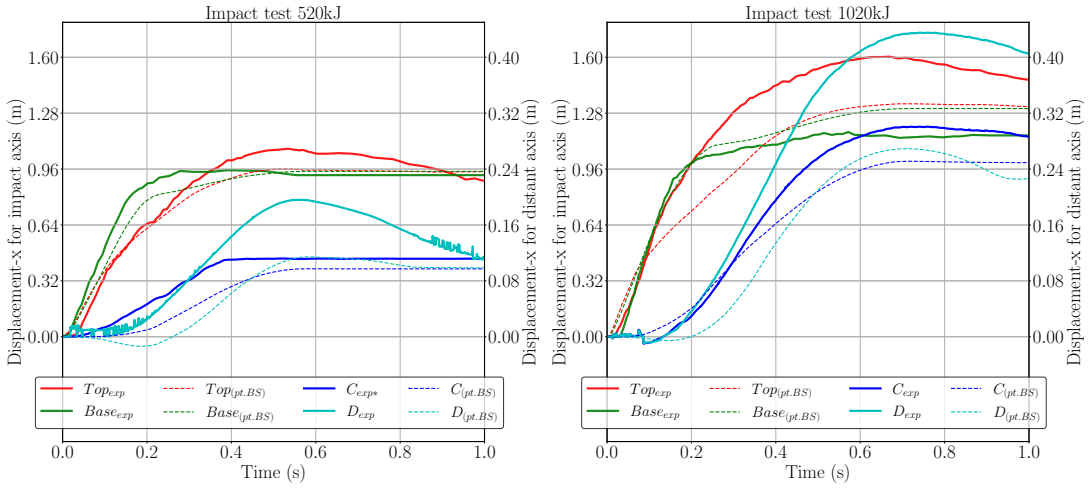

(a) (b)

Figure 20: Comparison of experimental displacement response with the NSCD model response obtained from the 'point' Base calibration set from 520kJ for (a) 520 kJ and (b) 1020kJ impact test

The successful model calibration also justified the usage of the Bayesian interface approach in place of a manual model calibration where some emphasis is typically given to a particular point and/or particular time instance. In case the model is to be calibrated based on a simplest approach, such as Monte Carlo simulations, would fail in satisfactorily describing the complex spatio-temporal response of the structure. Besides, these procedures do not provide the distribution of the calibrated parameters which help in understanding the uncertainty in calibration and also the possibility of finding more than one calibration set. This limitations justify considering an extensive stochastic calibration approach through Bayesian interface.

5.2. Model efficacy

The five model parameters are calibrated so that the simulation results conformed with the eight displacement evolution experimental database describing the spatio-temporal response of the structure when exposed to two impacts with different kinetic energies (520 and 1020 kJ). This way to proceed is particularly well adapted for this model for which parameter values can not be precisely measured or determined a priori. The model parameter e can not be directly compared to a measurable mechanical characteristic. Besides, the contact disk position is a parameter associated with the approach considered for modeling the connectors passing through the blocks. Also, the uncertainty and variability associated with the vertical play and friction angles justify such a calibration approach. This calibration approach, which makes use of PCE based meta-model, could advantageously be used for calibrating any relevant model where parameters cannot be precisely determined a priori.

The other asset of this calibration approach is that the best set of model parameters is defined from a quantitative evaluation of the deviation of the simulation results with the experimental data. When considering many output data, model parameters calibration most often relies on a qualitative evaluation of the simulated response with time, without any quantification of the deviation. By contrast, the proposed calibration approach guaranties that the set of determined parameter values is the optimal for describing the structure response with time and space.

Also, the presented simple NSCD model has limited assumptions and is immune to the bias of a typical FE model definition (constitutive laws, interface properties and so on) making the complex calibration procedure reliable. Besides, the combination of the meta-model and Bayesian interface presented a practical route to surpass the computational time constraint. The average computational time of a NSCD model simulation is about 20 minutes. Thereby, the initial investment in the stochastic analysis is 300 NSCD model runs to retrieve the essential database. In addition, a similar numerical modeling conducted by Furet et al. [27] using the finite element based software reported the computation time of 10 hours for one simulation. This highly significant difference further highlights the practical implementation potential of the NSCD model given the output of interest.

5.3. Energy dissipation

Estimating the energy dissipative capacities of the protective structures exposed to a localized dynamic loading is of paramount importance for understanding their mechanical response and improving their

design. Numerous research related to rockfall protection have considered the energy issue based on simulation results, with application to flexible barriers [66, 67, 68], embankments and walls [14, 27] and dissipative materials or components [69, 70, 71]. The provided data mainly aimed at explaining how the incident block kinetic energy is transferred and dissipated in the impacted structure and its foundation.

As for articulated concrete blocks structures, finite difference numerical simulations presented in [27] suggested that 50% of the projectile kinetic energy is dissipated by concrete plasticization due to shear and tension. The NSCD model proposed in the present study accounts for energy dissipation via e, μ_{cc} and μ_{cs}. The former indirectly accounted for damage to concrete blocks, while the two latter accounted for dissipation by friction between structure components. From the Bayesian interace results, it is evident that different sets of model parameters could result in very similar results, in particular when focusing on some specific locations of the structure. Ratios up to two are observed between parameter values from one calibrated model to the other, including the parameters governing energy dissipation (e, μ_{cc} and μ_{cs}). Obviously, the difference in model parameters has an influence on the contribution of each dissipative mechanism.

In the end, this highlights that simulation results interpreted in terms of energy dissipation should be considered with caution. The contribution by the various dissipative mechanisms (plasticization, friction...) strongly depends on the modeling strategy, on the constitutive laws and on the value attributed to the model parameters. This comes in addition to the classical energy conservation issue associated with some numerical schemes. These general but critical comments undoubtedly holds for any numerical model of structures exposed to dynamic loading, such as rockfall protective structures (e.g. [14, 27, 66, 68]). Further investigation is necessary for evaluating the influence of the model parameters on the contribution by each mechanisms to energy dissipation.

6. Conclusions and perspectives

In this work, a numerical model of a structure consisting of concrete blocks connected one to the others via metallic components and designed to intercept rockfall is presented and successfully calibrated. The model is kept simple and developed in Siconos software package based on NSCD approach for computation time saving purpose. NSCD revealed efficient for modeling such a complex structure where many components interact one with each other and some are invisible to each others. Each component

in the real structure is directly and indirectly reproduced in the NSCD model considering the interaction mechanisms and the design framework of objects with contactors in SICONOS. An average computation time of 20 mins is reported for the NSCD model in comparison to highly expensive FEM computations lasting for about 10 hours for the same computation.

Five model parameters required calibration. Three parameters governed the mechanical interaction between the various model components and two concerned the structure description. The calibration of these five model parameters is conducted based on the displacement with time at four different locations in the structure measured during real-scale experiments considering two projectile kinetic energies. The calibration is conducted considering Bayesian interface statistical learning method, accompanied by the meta-modeling techniques. This is done in view of accounting for the spatial and temporal displacement response of the structure upon a projectile impact. The meta-modeling techniques presented a surrogate of the NSCD model which represented the similar response albeit negligible computation time (microseconds) in comparison to the approximated 20 minutes time for one NSCD model computation. Subsequently, the large number of model computations are made possible by meta-models for the efficient usage of Bayesian interface for model calibration. Besides, the Sobol sensitivity analysis is made possible through the surrogate model which presented the relative influence of one parameter to the other both in space and time.

In the calibration process different calibration approaches, ranging from local point to the global structure's response are presented. It is evidenced that the model parameters value significantly depended on the calibration strategy, meaning on the number and variety of data used in this purpose. The final set of parameters value is reported to nearly mimic the spatial-temporal response of the real structure for both impact tests. An overall quantitative deviation of numerical results with the experimental evolution is reported to be 8.6% for the impact axis and 5.6% for the distant axis.

As a perspective, the developed NSCD model will be used to investigate the response of articulated concrete blocks structures when exposed to impacts under different conditions, in view of quantifying their real efficiency, in a similar approach as in Mentani et al. [72], Toe et al. [29] and Lambert et al. [30].

Acknowledgment

This work is conducted in the frame of the SMART PROTECT research project, leaded by Géolithe with INRAe, INRIA and Myotis as partners and is funded by the Auvergne-Rhône-Alpes region. The authors would like to thank Dr Emilie Rouzies for her valuable assistance and helpful comments with statistical learning methods.

References

[1] M. Jean, J. J. Moreau, Dynamics in the presence of unilateral contacts and dry friction: a numerical approach, in: G. Del Pietro, F. Maceri (Eds.), Unilateral problems in structural analysis. II, CISM 304, Spinger Verlag, 1987, pp. 151–196.

[2] M. Jean, The non smooth contact dynamics method, Computer Methods in Applied Mechanics and Engineering 177 (1999) 235–257. Special issue on computational modeling of contact and friction, J.A.C. Martins and A. Klarbring, editors.

[3] F. Dubois, V. Acary, M. Jean, The Contact Dynamics method: A nonsmooth story , Comptes Rendus Mécanique 346 (2018) 247–262.

[4] V. Acary, B. Brogliato, Numerical methods for nonsmooth dynamical systems. Applications in mechanics and electronics., Lecture Notes in Applied and Computational Mechanics 35. Berlin: Springer. xxi, 525 p. , 2008.

[5] V. Acary, M. Jean, Numerical simulation of monuments by the contact dynamics method, in: DGEMN-LNEC-JRC (Ed.), Monument-98, Workshop on seismic perfomance of monuments, Laboratório Nacional de engenharia Civil (LNEC), Lisboa, Portugal, Lisbon, Portugal, 1998, pp. 69–78. URL: https://hal.inria.fr/inria-00425359.

[6] V. Acary, J. Blaise, P. Drap, M. Florenzano, S. Garrec, M. Jean, D. Merad, Nscd method applied to mechanical simulation of masonry in historical buildings using moma, in: International Symposium WG3—Simple methods for architectural photogrammetry, 1999, pp. 1–8.

[7] A. Rafiee, M. Vinches, C. Bohatier, Application of the nscd method to analyse the dynamic behaviour of stone arched structures, International Journal of Solids and Structures 45 (2008) 6269–6283.

729 [8] F. Radjai, M. Jean, J. J. Moreau, S. Roux, Force Distributions in Dense Two-Dimensional Granular
730 Systems, Physical Review Letters 77 (1996) 274 – 277.

731 [9] M. Jean, V. Acary, Y. Monerie, Non-smooth contact dynamics approach of cohesive materials,
732 Philosophical Transactions of the Royal Society of London Series A Mathematical and Physical
733 Sciences (1934-1990) 359 (2001) 2497–2518.

734 [10] F. Bourrier, V. Acary, Predictive Capabilities of 2D and 3D Block Propagation Models Integrating
735 Block Shape Assessed from Field Experiments, Rock Mechanics and Rock Engineering 55 (2022)
736 591–609.

737 [11] N. Akhadkar, V. Acary, B. Brogliato, Multibody systems with 3D revolute joints with clearances:
738 an industrial case study with an experimental validation, Multibody System Dynamics 42 (2018)
739 249–282.

740 [12] M. Jean, G. Touzot, Implementation of unilateral contact and dry friction in computer codes dealing
741 with large deformations problems., Journal of theoritical and applied Mechanics (1988) 145–160.

742 [13] M. Wronski, M. Jean, Some computational aspects of structural dynamics problems with frictional
743 contact, Contact Mechanics (1995) 137–144.

744 [14] C. Ronco, C. Oggeri, D. Peila, Design of reinforced ground embankments used for rockfall protection,
745 Natural Hazards and Earth System Science (2009).

746 [15] M. Simmons, S. Pollak, B. Peirone, High energy rock fall embankment constructed using a free-
747 standing woven wire mesh reinforced soil structure, in: 60th Highway Geology Symposium, 2009,
748 pp. 290–301.

749 [16] S. Lambert, F. Bourrier, Design of rockfall protection embankments: A review, Engineering Geology
750 154 (2013) 77–88.

751 [17] O. Korini, M. Bost, J.-P. Rajot, Y. Bennani, N. Freitag, The influence of geosynthetics design on the
752 behavior of reinforced soil embankments subjected to rockfall impacts, Engineering Geology (2021).

753 [18] N. T. K. Lam, A. C. Y. Yong, C. Lam, J. S. H. Kwan, J. S. Perera, M. M. Disfani, E. Gad,
754 Displacement-based approach for the assessment of overturning stability of rectangular rigid barriers
755 subjected to point impact, Journal of Engineering Mechanics (2018).

[19] A. Yong, C. Lam, N. Lam, J. Perera, J. Kwan, Analytical solution for estimating sliding displacement of rigid barriers subjected to boulder impact, Journal of Engineering Mechanics (2019).

[20] M. Çelik, Investigating the performance of passageway corridor for ground reinforced embankments against rockfall , Journal of Mountain Science (2023).

[21] T. Colgan, E. Ewe, Design of a large scale rockfall protection bund for coastal transport corridor recovery following the 2016 kaikōura earthquake, in: Pacific conference on earthquake engineering, 2019, pp. 1–12.

[22] R. Green, J. S. Finlan, Rapid Design of a Modular Rockfall Protection Wall in Response to the 2016 KaiKoura Earthquake, 2021, pp. 151–165. doi:10.1061/9780784483688.015.

[23] J. P. Perera, N. Lam, Rockfall protection wall that can withstand multiple strikes without needing to be repaired, International Journal of Impact Engineering 173 (2023) 104476.

[24] S. Lambert, F. Bourrier, P. Gotteland, F. Nicot, An experimental investigation of the response of slender protective structures to rockfall impacts, Canadian geotechnical journal (2019).

[25] C. Williams, J. Morkeh, K. Dorfschmidt, C. Poon, P. Matlashewski, J. Carvalho, Innovative rockfall solutions based on calibration and field testing, Mining, Metallurgy & Exploration (2021).

[26] A. Furet, S. Lambert, P. Villard, J. P. Jarrin, J. Lorentz, Response of rockfall protection walls subjected to impact, Revue française de géotechnique (2020).

[27] A. Furet, S. Lambert, P. Villard, J. J. Philippe, Experimental and numerical impact responses of an innovative rockfall protection structure made of articulated concrete blocks , Rock Mechanics and Rock Engineering (2022).

[28] F. Bourrier, S. Lambert, J. Baroth, A reliability-based approach for the design of rockfall protection fences , Rock Mechanics and Rock Engineering (2015).

[29] D. Toe, A. Mentani, L. Govoni, F. Bourrier, G. Gottardi, S. Lambert, Introducing meta-models for a more efficient hazard mitigation strategy with rockfall protection barriers, Rock Mechanics and Rock Engineering (2018).

[30] S. Lambert, D. Toe, A. Mentani, F. Bourrier, A Meta-Model-Based Procedure for Quantifying the On-Site Efficiency of Rockfall Barriers, Rock Mechanics and Rock Engineering 54 (2021) 487–500.

[31] V. Acary, F. Perignon, Siconos: A Software Platform for Modeling, Simulation, Analysis and Control of Nonsmooth Dynamical Systems, SIMULATION NEWS EUROPE, ArgeSIM/ASIM 17 (2007) 19–26.

[32] V. Acary, O. Bonnefon, M. Brémond, O. Huber, S. Sinclair, V. Acary, O. Bonnefon, M. Brémond, O. Huber, F. Pérignon, V. Acary, O. Bonnefon, M. Brémond, O. Huber, An introduction to Siconos, Technical report (2019).

[33] V. Acary, Energy conservation and dissipation properties of time-integration methods for nonsmooth elastodynamics with contact, Journal of Applied Mathematics and Mechanics / Zeitschrift für Angewandte Mathematik und Mechanik 96 (2016) 585–603.

[34] J. Escallón, C. Wendeler, E. Chatzi, P. Bartelt, Parameter identification of rockfall protection barrier components through an inverse formulation, Engineering Structures 77 (2014) 1–16.

[35] D. Rossat, J. Baroth, M. Briffaut, F. Dufour, A. Monteil, B. Masson, S. Michel-Ponnelle, Bayesian inference with correction of model bias for thermo-hydro-mechanical models of large concrete structures, Engineering Structures 278 (2023) 115433.

[36] M. B. Heredia, N. Eckert, C. Prieur, E. Thibert, Bayesian calibration of an avalanche model from autocorrelated measurements along the flow: application to velocities extracted from photogrammetric images, Journal of Glaciology 66 (2020) 373–385.

[37] M. Asch, M. Bocquet, M. Nodet, Data Assimilation, Society for Industrial and Applied Mathematics, Philadelphia, PA, 2016. URL: https://epubs.siam.org/doi/abs/10.1137/1.9781611974546. doi:10.1137/1.9781611974546. arXiv:https://epubs.siam.org/doi/pdf/10.1137/1.9781611974546.

[38] M. A. Hariri-Ardebili, B. Sudret, Polynomial chaos expansion for uncertainty quantification of dam engineering problems, Engineering Structures 203 (2020) 109631.

[39] X. Guo, D. Dias, C. Carvajal, L. Peyras, P. Breul, Reliability analysis of embankment dam sliding stability using the sparse polynomial chaos expansion, Engineering Structures 174 (2018) 295–307.

[40] R. Gupta, D. Rossat, X. Dérobert, J. Baroth, M. Briffaut, G. Villain, F. Dufour, Blind comparison

of saturation ratio profiles on large rc structures by means of ndt and sfe—application to the vercors mock-up, Engineering Structures 258 (2022) 114057.

[41] G. D. Saxce, Z. Q. Feng, New inequality and functional for contact with friction: The implicit standard material approach, Mechanics of Structures and Machines 19 (1991) 301–325.

[42] V. Acary, M. Brémond, O. Huber, Advanced Topics in Nonsmooth Dynamics., Acary, V. and Brüls. O. and Leine, R. (eds). Springer Verlag, 2018, p. 375–457.

[43] P. A. Cundall, O. D. Strack, A discrete numerical model for granular assemblies, geotechnique 29 (1979) 47–65.

[44] N. Bićanić, Discrete element methods, Encyclopedia of computational mechanics (2004).

[45] Q. Z. Chen, V. Acary, G. Virlez, O. Brüls, A nonsmooth generalized-α scheme for flexible multibody systems with unilateral constraints, International Journal for Numerical Methods in Engineering 96 (2013) 487–511.

[46] O. Brüls, V. Acary, A. Cardona, On the Constraints Formulation in the Nonsmooth Generalized-α Method, in: S. I. Publishing (Ed.), Advanced Topics in Nonsmooth Dynamics. Transactions of the European Network for Nonsmooth Dynamics, 2018, pp. 335–374. URL: https://hal.inria.fr/hal-01878550. doi:10.1007/978-3-319-75972-2_9.

[47] O. Brüls, V. Acary, A. Cardona, Simultaneous enforcement of constraints at position and velocity levels in the nonsmooth generalized-α scheme, Computer Methods in Applied Mechanics and Engineering 281 (2014) 131–161.

[48] T. Schindler, S. Rezaei, J. Kursawe, V. Acary, Half-explicit timestepping schemes on velocity level based on time-discontinuous Galerkin methods, Computer Methods in Applied Mechanics and Engineering 290 (2015) 250–276.

[49] T. Schindler, V. Acary, Timestepping schemes for nonsmooth dynamics based on discontinuous Galerkin methods: Definition and outlook, Mathematics and Computers in Simulation 95 (2014) 180–199.

[50] C. B. Barber, D. P. Dobkin, H. Huhdanpaa, The quickhull algorithm for convex hulls, ACM Trans. Math. Softw. 22 (1996) 469–483.

[51] EOTA, Ead 340059-00-0106: Falling rock protections kits, 2018.

[52] M. Taklas, M. Leblouba, S. Barakat, A. Fageeri, F. Mohamad, Concrete-to-concrete shear friction behavior under cyclic loading: experimental investigation, Scientific Reports 12 (2022) 9451.

[53] H. Niederreiter, 1. Monte Carlo Methods and Quasi-Monte Carlo Methods, 1992, pp. 1–12. URL: https://epubs.siam.org/doi/abs/10.1137/1.9781611970081.ch1. doi:10.1137/1.9781611970081.ch1. arXiv:https://epubs.siam.org/doi/pdf/10.1137/1.9781611970081.ch1.

[54] C. Lataniotis, S. Marelli, B. Sudret, UQLab user manual – The Input module, Technical Report, Chair of Risk, Safety & Uncertainty Quantification, ETH Zurich, 2015. Report UQLab-V0.9-102.

[55] S. Marelli, B. Sudret, UQLab: A Framework for Uncertainty Quantification in Matlab, 2014, pp. 2554–2563. doi:10.1061/9780784413609.257.

[56] I. M. Sobol, A screening design for factorial experiments with interactions, Mathematical and Computer Modelling 1 (1993) 407–414.

[57] B. Sudret, Global sensitivity analysis using polynomial chaos expansions, Reliability Engineering & System Safety 93 (2008) 964–979. Bayesian Networks in Dependability.

[58] E. Rouzies, C. Lauvernet, B. Sudret, A. Vidard, How to perform global sensitivity analysis of a catchment-scale, distributed pesticide transfer model? application to the peshmelba model, Geoscientific Model Development (under review).

[59] S. Marelli, C. Lamas, B. Sudret, UQLab user manual - sensitivity analysis, 2015. doi:10.13140/RG.2.1.1419.4404.

[60] S. Dobre, T. Bastogne, C. Profeta, M. Barberi-Heyob, A. Richard, Limits of variance-based sensitivity analysis for non-identifiability testing in high dimensional dynamic models, Automatica 48 (2012) 2740–2749.

[61] T. Bayes, n. Price, Lii. an essay towards solving a problem in the doctrine of chances. by the late rev. mr. bayes, f. r. s. communicated by mr. price, in a letter to john canton, a. m. f. r. s, Philosophical Transactions of the Royal Society of London 53 (1763) 370–418.

[62] Y. Marzouk, D. Xiu, A stochastic collocation approach to bayesian inference in inverse problems, Communications in Computational Physics (2009).

[63] Y. M. Marzouk, H. N. Najm, Dimensionality reduction and polynomial chaos acceleration of bayesian inference in inverse problems, Journal of Computational Physics 228 (2009) 1862–1902.

[64] L. Yan, L. Guo, Stochastic collocation algorithms using l_1-minimization for bayesian solution of inverse problems, SIAM Journal on Scientific Computing 37 (2015) A1410–A1435.

[65] P.-R. Wagner, J. Nagel, S. Marelli, B. Sudret, UQLab user manual – Bayesian inversion for model calibration and validation, Technical Report, Chair of Risk, Safety and Uncertainty Quantification, ETH Zurich, Switzerland, 2022. Report UQLab-V2.0-113.

[66] H. Xu, C. Gentilini, Z. Yu, X. Qi, S. Zhao, An energy allocation based design approach for flexible rockfall protection barriers, Engineering Structures 173 (2018) 831–852.

[67] L. Castanon-Jano, E. Blanco-Fernandez, D. Castro-Fresno, Design of a new energy dissipating device and verification for use in rockfall protection barriers, Engineering Structures 199 (2019) 109633.

[68] D. Di Giacinto, L. Grassia, G. Capriello, E. Ruocco, A novel steel damping system for rockfall protection galleries, Journal of Constructional Steel Research 175 (2020) 106360.

[69] L. Zhang, S. Lambert, F. Nicot, Discrete dynamic modelling of the mechanical behaviour of a granular soil, International Journal of Impact Engineering 103 (2017) 76–89.

[70] M. Previtali, M. O. Ciantia, S. Spadea, R. P. Castellanza, G. B. Crosta, Multiscale modelling of dynamic impact on highly deformable compound rockfall fence nets, Proceedings of the Institution of Civil Engineers - Geotechnical Engineering 174 (2021) 498–511.

[71] S. Yan, Y. Wang, D. Wang, S. He, Application of eps geofoam in rockfall galleries: Insights from large-scale experiments and fdem simulations, Geotextiles and Geomembranes 50 (2022) 677–693.

[72] A. Mentani, L. Govoni, G. Gottardi, S. Lambert, F. Bourrier, D. Toe, A new approach to evaluate the effectiveness of rockfall barriers, Procedia Engineering 158 (2016) 398–403. VI Italian Conference of Researchers in Geotechnical Engineering, CNRIG2016 - Geotechnical Engineering in Multidisciplinary Research: from Microscale to Regional Scale, 22-23 September 2016, Bologna (Italy).

[73] S. Marelli, B. Sudret, Uqlab user manual - polynomial chaos expansions, 2015. doi:10.13140/RG.2.1.3778.7366.

Appendix A. PCE based meta-model

Consider the articulated structure model represented by a $\mathcal{M}(\mathbf{X})$ as an equivalent mathematical model. Here, $\mathbf{X} \in \mathbb{R}^M$ is a random vector with independent components described by the joint probability density function (PDF) $f_{\mathbf{X}}$. Consider also a finite variance computational model as a map $Y = \mathcal{M}(\mathbf{X})$, with $Y \in \mathbb{R}$ such that:

$$\mathbb{E}\left[Y^2\right] = \int_{\mathcal{D}_{\mathbf{X}}} \mathcal{M}(\boldsymbol{x})^2 f_{\mathbf{X}}(\boldsymbol{x}) \mathrm{d}\boldsymbol{x} < \infty \tag{A.1}$$

Then, under the assumption of Equation A.1, the PCE of $\mathcal{M}(\mathbf{X})$ is defined as:

$$Y = \mathcal{M}(\mathbf{X}) = \sum_{\boldsymbol{\alpha} \in \mathbb{N}^M} y_{\boldsymbol{\alpha}} \Psi_{\boldsymbol{\alpha}}(\mathbf{X}) \tag{A.2}$$

where, the $\Psi_{\boldsymbol{\alpha}}(\mathbf{X})$ are multivariate polynomials orthonormal with respect to $f_{\mathbf{X}}$, $\alpha \in \mathbb{N}^M$ is a multi-index that identifies the components of the multivariate polynomials $\Psi_{\boldsymbol{\alpha}}$ and the $y_\alpha \in \mathbb{R}$ are the corresponding coefficients. In practical applications, the sum in Equation A.2 needs to be truncated to a finite sum by introducing the truncated polynomial chaos expansion:

$$\mathcal{M}(\mathbf{X}) \approx \mathcal{M}^{PC}(\mathbf{X}) = \sum_{\boldsymbol{\alpha} \in \mathcal{A}} y_{\boldsymbol{\alpha}} \Psi_{\boldsymbol{\alpha}}(\mathbf{X}) \tag{A.3}$$

where, $\mathcal{A} \subset \mathbb{N}^M$ is the set of selected multi-indices of multivariate polynomials.

In this work, the least-angle regression (LARS) method is used to create the PCE meta-model truncated to the maximum polynomial degree (p) ranging from 1 to 20, and using hyperbolic truncation scheme (q) ranging from 0.5 to 1.

$$\mathcal{A}^{M,p,q} = \{\boldsymbol{\alpha} \in \mathcal{A}^{M,p} \ : \ \|\boldsymbol{\alpha}\|_q \leqslant p\}, \ where \ , \|\boldsymbol{\alpha}\|_q = \left(\sum_{i=1}^{M} \alpha_i^q\right)^{1/q} \tag{A.4}$$

The accuracy of the constructed PCE is estimated by computing the leave-one-out (LOO) cross-validation error (ϵ_{LOO}). It consists in building N meta-models $\mathcal{M}^{PC\setminus i}$, each one created on a reduced experimental design $\mathfrak{X}\setminus\mathbf{x}^{(i)} = \{\mathbf{x}^{(j)}, j = 1, ..., N, j \neq i\}$ and comparing its prediction on the excluded point $\mathbf{x}^{(i)}$ with the real value $y^{(i)} = \mathcal{M}\big(\mathbf{x}^{(i)}\big)$ [73]. The leave-one-cross-validation error can be written as:

$$\epsilon_{LOO} = \frac{\sum_{i=1}^{N} \left(\mathcal{M}\big(\mathbf{x}^{(i)} - \mathcal{M}^{PC\setminus i}\big(\mathbf{x}^{(i)}\big)\right)^2}{\sum_{i=1}^{N} \left(\mathcal{M}\big(\mathbf{x}^{(i)} - \hat{\mu}_Y\right)^2} \tag{A.5}$$

where, $\hat{\mu}_Y$ is the mean of the experimental design sample.

Appendix B. Bayesian interface for model calibration

Consider the computational model $\mathcal{M}$ that allows the analyst to predict certain quantities of interest gathered in a vector $\boldsymbol{y} \in \mathbb{R}^{N_{out}}$ as a function of input parameters $\boldsymbol{x}$:

$$\mathcal{M} : \boldsymbol{x} \in \mathcal{D}_{\mathbf{X}} \subset \mathbb{R}^M \mapsto \boldsymbol{y} = \mathcal{M}(x) \in \mathbb{R}^{N_{out}} \tag{B.1}$$

The Bayesian interface for model calibration focus on identifying the input parameters of a computational model to recover the observations in the collected output data-set. It comprises of a computational forward model $\mathcal{M}$, a set of input parameters $\boldsymbol{x} \in \mathcal{D}_{\mathbf{X}}$ that need to be inferred, and a set of experimental data $\mathcal{Y}$. Here, $\mathcal{Y} \overset{\text{def}}{=} \{\boldsymbol{y}_1, ..., \boldsymbol{y}_N\}$ is a global data set of N independent measured quantities of interest $(\boldsymbol{y}_i)$.

The forward model $\boldsymbol{x} \mapsto \mathcal{M}(x)$ is a mathematical representation of the system under consideration. The lack of knowledge on the input parameters is modeled by considering them as a random vector, denoted by $\boldsymbol{X}$ which is assumed to follow a so-called prior distribution (with support $\mathcal{D}_{\boldsymbol{X}}$), as presented in Figure 12 in the present work.

$$\boldsymbol{X} \sim \pi(\boldsymbol{x}) \tag{B.2}$$

The Bayesian statistics combines this prior knowledge on the parameters with the few observed data points to obtain a statistical model called posterior distribution ($\pi(\boldsymbol{x} \mid \boldsymbol{y})$) of the input parameters, using Bayes' theorem [61], expressed as:

$$\pi(\boldsymbol{x} \mid \boldsymbol{y}) = \frac{\pi(\boldsymbol{y} \mid \boldsymbol{x})\pi(\boldsymbol{x})}{\pi(\boldsymbol{y})} \tag{B.3}$$

Now, considering the available data set $(\mathcal{Y})$ as independent realizations of $\boldsymbol{Y} \mid \boldsymbol{x} \sim \pi(\boldsymbol{y} \mid \boldsymbol{x})$, the collected measurements result in the definition of the likelihood function $\mathcal{L}(\boldsymbol{x}; \mathcal{Y})$, which is a function of input parameters $\boldsymbol{x}$:

$$\mathcal{L} : \boldsymbol{x} \mapsto \mathcal{L}(\boldsymbol{x}; \mathcal{Y}) \overset{\text{def}}{=} \prod_{i=1}^{N} \pi(\boldsymbol{y}_i \mid \boldsymbol{x}) \tag{B.4}$$

This implicitly assumes independence between individual measurements in $\mathcal{Y}$. Intuitively the likelihood function for a given $\boldsymbol{x}$ returns the relative likelihood of observing the data at hand, under the assumption that it follows the prescribed parametric distribution $\pi(\boldsymbol{y} \mid \boldsymbol{x})$.

As all models are simplification of the real world, a discrepancy term (ϵ) is introduced to connect real world observations ($\mathcal{Y}$) to the predictions by the model. In practice, the discrepancy term represents the effects of the measurement error and model inaccuracy. The discrepancy term introduced here reads:

$$\boldsymbol{y} = \mathcal{M}(x) + \epsilon \tag{B.5}$$

Here, the ϵ is assumed as an additive Gaussian discrepancy [65] with a zero mean and given covariance matrix ($\boldsymbol{\Sigma}$):

$$\epsilon \sim \mathcal{N}(\epsilon \mid \mathbf{0}, \boldsymbol{\Sigma}) \tag{B.6}$$

Taking insights from the discrepancy term definition, a particular measurement point ($\boldsymbol{y}_i \in \mathcal{Y}$, is a realization of the Gaussian distribution with mean value $\mathcal{M}(x)$ and covariance matrix $\boldsymbol{\Sigma}$. This distribution is named as discrepancy model and is expressed as:

$$\pi(\boldsymbol{y} \mid \boldsymbol{x}) = \mathcal{N}(\boldsymbol{y} \mid \mathcal{M}(\boldsymbol{x}), \boldsymbol{\Sigma}) \tag{B.7}$$

In application, the discrepancy model defines the connection between the supplied data ($\mathcal{Y}$) and the forward model. In the present work, as the model calibration relies on a single experimental measurement, the discrepancy model with known residual variance is assigned.

Afterwards, the N independent available measurements gathered in the data-set $\mathcal{Y}$ are used to define the likelihood function as:

$$\begin{aligned} \mathcal{L}(\boldsymbol{x}; \mathcal{Y}) &= \prod_{i=1}^{N} \mathcal{N}(\boldsymbol{y}_i \mid \mathcal{M}(\boldsymbol{x}), \boldsymbol{\Sigma}) \\ &= \prod_{i=1}^{N} \frac{1}{\sqrt{(2\pi)^{N_{out}} \det(\boldsymbol{\Sigma})}} \exp\left(-\frac{1}{2} \Big(\boldsymbol{y}_i - \mathcal{M}(\boldsymbol{x})\Big)^{\intercal} \boldsymbol{\Sigma}^{-1} \Big(\boldsymbol{y}_i - \mathcal{M}(\boldsymbol{x})\Big) \right) \end{aligned} \tag{B.8}$$

Moreover, in the present work, the experimental data is retrieved through various points and for different impact energies (*i.e.*, $\mathcal{Y} = \{\boldsymbol{y}_1, ..., \boldsymbol{y}_N\}$). The Bayesian interface allows to incorporate all these data points together for the model calibration by arranging the elements of $\mathcal{Y}$ in disjoint data-groups and define different likelihood functions for each data group [65].

Denoting the g-th data group by $\mathcal{G}^g = \{\boldsymbol{y}_i\}_{i \in \boldsymbol{u}}$, where $\boldsymbol{u} \subseteq \{1, ..., N\}$, the full data-set can be combined by

$$\mathcal{Y} = \bigcup_{g=1}^{N_{gr}} \mathcal{G}^{(g)} \tag{B.9}$$

Here, each of the N_{gr} data groups contains measurements collected at the same measurement point. In the context of present work, these measurements are experimental data recorded at 'init', 'max' and 'rest' time instances at a particular point. This makes it evident to have a different likelihood function $\mathcal{L}^{(g)}$ describing the experimental conditions that led to measuring $\mathcal{G}^{(g)}$. Assuming the Independence between N_{gr} measurement conditions, the full likelihood function can then be written as

$$\mathcal{L}(\boldsymbol{x}_{\mathcal{M}}, \boldsymbol{x}_{\epsilon}; \mathcal{Y}) = \prod_{g=1}^{N_{gr}} \mathcal{L}^{(g)}(\boldsymbol{x}_{\mathcal{M}}, \boldsymbol{x}_{\epsilon}^{(g)}; \mathcal{G}^{(g)}) \tag{B.10}$$

where, $\boldsymbol{x}_{\epsilon}^{(g)}$ are the parameters of the g-th discrepancy group. The different model output groups are assigned through a model output map (MOMap) vector [65].

Thereby, following the Bayes' theorem, the posterior distribution $\pi(\boldsymbol{x} \mid \mathcal{Y})$ of the parameters $(\boldsymbol{x})$ given the observations in $\mathcal{Y}$ can be written as:

$$\pi(\boldsymbol{x} \mid \mathcal{Y}) = \frac{\mathcal{L}(\boldsymbol{x}; \mathcal{Y})\pi(\boldsymbol{x})}{Z} \tag{B.11}$$

Here, Z is a normalizing factor, known as the marginal likelihood or evidence, is added to ensure that this distribution integrates to 1:

$$Z \stackrel{\text{def}}{=} \int_{\mathcal{D}_{\boldsymbol{X}}} \mathcal{L}(\boldsymbol{x}; \mathcal{Y})\pi(\boldsymbol{x}) \mathrm{d}\boldsymbol{x} \tag{B.12}$$

The closed form solutions do not exist in practice the posterior distribution is obtained through Markov chain Monte Carlo (MCMC) simulations. In the present work, among many proposed algorithms in [65], the Adaptive Metropolis (AM) algorithm is used and 100 parallel chains with 1000 steps are assigned to the MCMC solver. The start of the covariance adaptation in AM algorithm is assigned at 100th step (see Wagner et al. [65] for more details).

The output $(\boldsymbol{y})$ predictive capabilities of the Bayesian interface is assessed through the comparison of prior $(\pi(\boldsymbol{y}))$ and posterior $(\pi(\boldsymbol{y} \mid \mathcal{Y}))$ output distributions as:

$$\pi(\boldsymbol{y}) = \int_{\mathcal{D}_{\boldsymbol{X}}} \pi(\boldsymbol{y} \mid \boldsymbol{x}) \pi(\boldsymbol{x}) \mathrm{d}\boldsymbol{x} \tag{B.13}$$

$$\pi(\boldsymbol{y} \mid \mathcal{Y}) = \int_{\mathcal{D}_{\boldsymbol{X}}} \pi(\boldsymbol{y} \mid \boldsymbol{x}) \pi(\boldsymbol{x} \mid \mathcal{Y}) \mathrm{d}\boldsymbol{x} \tag{B.14}$$

Lastly, in the present studies, the purpose of Bayesian interface is to obtain the 'best set of input parameters'. Given the posterior distribution ($\pi(\boldsymbol{x} \mid \mathcal{Y})$), we are interested in finding a suitable set among the posterior computed set *i.e.,* $\boldsymbol{X} \mid \mathcal{Y}$. This is done through a point estimator ($\hat{\boldsymbol{x}}$) computed from:

$$\pi(\boldsymbol{y} \mid \mathcal{Y}) \overset{\text{def}}{=} \pi(\boldsymbol{y} \mid \hat{\boldsymbol{x}}) \tag{B.15}$$

This point estimator can be a mean or mode (maximum a posteriori 'MAP') [65] of the posterior distribution as per user's choice.